AD-A136 930 EFFECTS OF MULTIPLE CYLINDERS ON THE FORMATION OF VON KARMAN VORTEX STREETS(U) AIR FORCE INST OF TECH WRIGHT-PATTERSON AFB OH SCHOOL OF ENGI.. G F CLARK 1/2

UNCLASSIFIED DEC 83 AFIT/GAE/ENY/83D-5 F/G 20/4 NL

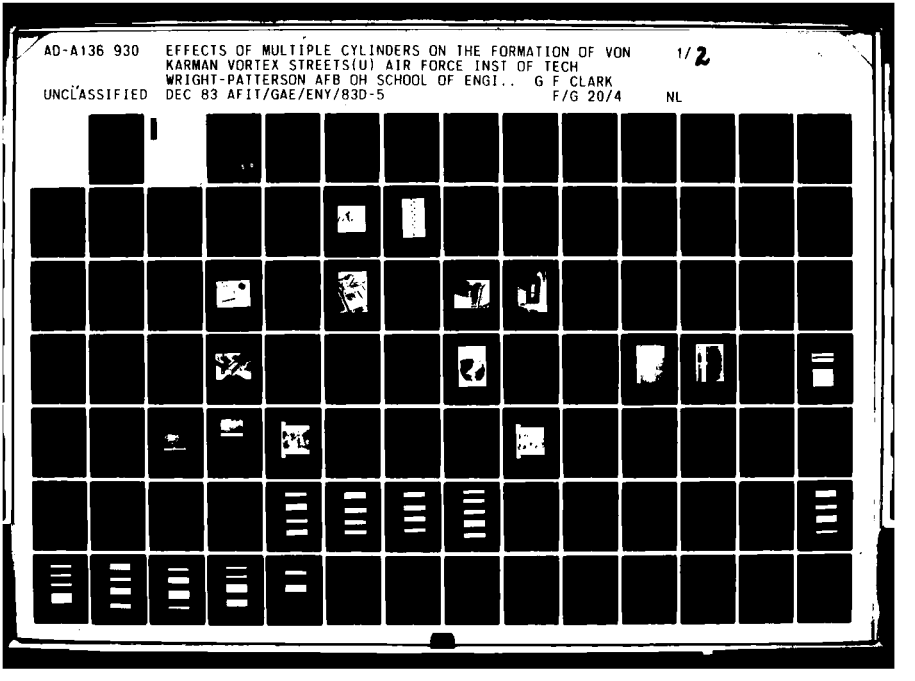

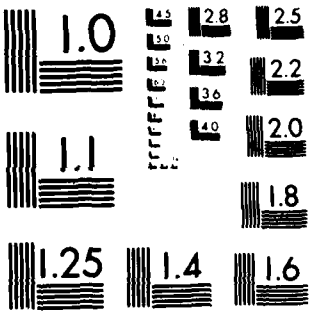

MICROCOPY RESOLUTION TEST CHART
NATIONAL BUREAU OF STANDARDS 1963-A

AFIT/GAE/ENY/83D-5

EFFECTS OF MULTIPLE CYLINDERS ON THE FORMATION OF VON KÁRMÁN VORTEX STREETS

THESIS

Gary F. Clark
Captain, USAF

AFIT/GAE/ENY/83D-5

DTIC
ELECTE
JAN 1 8 1984
S D
E

Approved for public release; distribution unlimited

AFIT/GAE/ENY/83D-5

EFFECTS OF MULTIPLE CYLINDERS ON THE FORMATION OF VON KÁRMÁN VORTEX STREETS

THESIS

Presented to the Faculty of the School of Engineering

of the Air Force Institute of Technology

Air University

In Partial Fulfillment of the

Requirements for the Degree of

Master of Science in Aeronautical Engineering

DTIC COPY INSPECTED

Gary F. Clark, B.S.

Captain, USAF

December 1983

Accession For
NTIS GRA&I
DTIC TAB
Unannounced
Justification
By
Distribution/
Availability Codes
Dist | Avail and/or Special
A-1

Approved for public release; distribution unlimited

Preface

The absence of rows of von Kármán vortex streets in schlieren photographs taken of flow over multiple cylinders sparked this effort to determine what effect multiple cylinders have on this phenomenon, and thus, why it did not occur. Answers to these questions can then be used to design a turbulence grid for future laser beam degradation work. I hope that my work may stimulate further theoretical and experimental research in this field.

I would like to thank the many support individuals of the AFIT Model Shop and the Aeronautics Department Laboratory who rendered exact and timely assistance throughout this research. Also, my appreciation goes to Maj (Dr.) Eric Jumper, Dr. William Elrod, and Capt (Dr.) Wesley Cox who supplied valuable guidance when all appeared lost. Most of all, I thank my wife, Rita, and son, Michael, who endured and sacrificed so much for this research.

Gary F. Clark

Table of Contents

	Page
Preface	ii
List of Figures	v
List of Tables	viii
List of Symbols	ix
Abstract	x
I. Introduction	1
II. Theory and Approach	3
Periodic Flow Field Creation	3
Visualization of Flow Field Structure	9
Flow Field Measurement	10
III. Experimental Apparatus	15
Water Table	15
Free Jet	18
IV. Experimental Procedure	27
Water Tunnel	27
Free Jet Schlieren Photography	29
Free Jet Velocity Fluctuation Measurement	29
V. Results and Discussion of Results	33
Water Flow Field	33
Free Jet Flow Field	34
VI. Conclusions	52
VII. Recommendations	54
Appendix A: Modifications Made to the Cylinder and Free Jet Nozzle	55
Appendix B: Hot Film Measurements for the Single Cylinder Extended 1.905 cm from the Jet Exit Plane	59

Page

Appendix C: Hot Film Measurements of the von Karman Vortex Street 68

Bibliography 81

Vita 83

List of Figures

Figure		Page
1.	Strouhal Number as a Function of Reynolds Number (Ref 10: 32)	3
2.	Compressible Vortex Street, M = .556, $Re_D = 2.7 \times 10^5$ (Ref 2: 109)	5
3.	Vortex Street in Water, $Re_D = 105$ (Ref 11: 57)	6
4.	Von Kármán Vortex Street, $Re_D > 40$ (After Refs 4: 816 and 2: 113)	8
5.	Turbulence Signals. (a) Sine Wave Plus Random Noise. (b) Narrow-Band Random Noise. (c) Wide-Band Random Noise (Ref 13: 17)	12
6.	Autocorrelation Functions of Turbulent Signals. (a) Sine Wave Plus Random Noise. (b) Narrow-Band Random Noise. (c) Wide-Band Random Noise (Ref 13: 21)	13
7.	Power Spectral Density Plots. (a) Sine Wave Plus Random Noise. (b) Narrow-Band Random Noise. (c) Wide-Band Random Noise (Ref 13: 24)	14
8.	Flow Injection Device and Circular Cylinder Model	17
9.	Water Tunnel and Overhead Projection Arrangement	19
10.	1.905 cm Spacers, Free Jet Rectangular Nozzle, and Helium Injection Cylinder Arrangement	21
11.	Helium Injection Cylinder Attached to the Rectangular Nozzle	22
12.	Schlieren Photography System Arrangement	24
13.	Hot Film Statistical Measurement Arrangement	25
14.	Hot Film Positioned in the Channel Flow Field of the 5 cm by 5 cm Nozzle	31
15.	Von Kármán Vortex Street with Turbulence in the Water Tunnel, $Re_D = 9.95 \times 10^2$	35

Figure Page

16. Schlieren Photograph of Wake Pattern for 4 Diameters Separation at M = .6 38

17. Schlieren Photograph of Helium Injection Cylinder Flow at M = .1 39

18. Schlieren Photographs Comparing Flow Fields (a) With and (b) Without Spacers, M = .6 41

19. Power Spectral Density Plots of Single Cylinder Wake Pattern Using Spacers, M = .1 (TP 9 - TP 12) . 43

20. Schlieren Photograph of Single Cylinder Flow Field Using the Square Nozzle and 1.27 cm Spacers, M = .6 44

21. Schlieren Photograph of Single Cylinder Flow Field Using the Square Nozzle and the Reversed Bracket Mounting, M = .6 45

22. Schlieren Photograph of von Kármán Vortex Street, M = .6 46

23. Power Spectral Density Plots of von Kármán Vortex Street at M = .1 (TP 1 - TP 4) 48

24. Schlieren Photograph of Two von Kármán Vortex Streets at M = .6 50

25. Cylinder Modifications. (a) Chopped Cylinder, (b) Flat Plate 56

26. Autocorrelation Functions for the Single Cylinder in the Free Jet Flow Field at M = .1 (TP 1 - TP 4) 60

27. Autocorrelation Functions for the Single Cylinder in the Free Jet Flow Field at M = .1 (TP 5 - TP 8) 61

28. Autocorrelation Functions for the Single Cylinder in the Free Jet Flow Field at M = .1 (TP 9 - TP 12) 62

29. Autocorrelation Functions for the Single Cylinder in the Free Jet Flow Field at M = .1 (TP 13 - TP 17) 63

Figure Page

30. Power Spectral Density Plots for the Single Cylinder in the Free Jet Flow Field at M = .1 (TP 1 - TP 4) 64

31. Power Spectral Density Plots for the Single Cylinder in the Free Jet Flow Field at M = .1 (TP 5 - TP 8) 65

32. Power Spectral Density Plots for the Single Cylinder in the Free Jet Flow Field at M = .1 (TP 9 - TP 12) 66

33. Power Spectral Density Plots for the Single Cylinder in the Free Jet Flow Field at M = .1 (TP 13 - TP 17) 67

34. Autocorrelation Functions for the von Kármán Vortex Street at M = .1 (TP 1 - TP 4) 69

35. Autocorrelation Functions for the von Kármán Vortex Street at M = .1 (TP 5 - TP 8) 70

36. Autocorrelation Functions for the von Kármán Vortex Street at M = .1 (TP 9 - TP 12) 71

37. Autocorrelation Functions for the von Kármán Vortex Street at M = .1 (TP 13 - TP 16) 72

38. Autocorrelation Functions for the von Kármán Vortex Street at M = .1 (TP 17 - TP 20) 73

39. Autocorrelation Functions for the von Kármán Vortex Street at M = .1 (TP 21 - TP 22) 74

40. Power Spectral Density Plots for the von Kármán Vortex Street at M = .1 (TP 1 - TP 4) 75

41. Power Spectral Density Plots for the von Kármán Vortex Street at M = .1 (TP 5 - TP 8) 76

42. Power Spectral Density Plots for the von Kármán Vortex Street at M = .1 (TP 9 - TP 12) 77

43. Power Spectral Density Plots for the von Kármán Vortex Street at M = .1 (TP 13 - TP 16) 78

44. Power Spectral Density Plots for the von Kármán Vortex Street at M = .1 (TP 17 - TP 20) 79

45. Power Spectral Density Plots for the von Kármán Vortex Street at M = .1 (TP 21 - TP 22) 80

List of Tables

Table		Page
I.	Nozzle/Cylinder Modifications	36
II.	Hot Film Measurement Test Points for Cylinder with Spacers	42
III.	Hot Film Measurement Test Points for von Kármán Vortex Street	47

List of Symbols

Symbol		Units
D	cylinder diameter	cm
G	power spectral density function	---
K	ratio of specific heats	---
M	Mach number	---
P_o	total pressure	kPa
P_e	static pressure	kPa
R	gas constant for air	joules/°K kg
R_c	autocorrelation coefficient	---
Re_D	Reynolds number based on cylinder diameter	---
S	Strouhal number	---
T	sample time	s
T_o	total temperature	°K
f	frequency	1/s
f_o	reference frequency	1/s
t	time	s
v	velocity	m/s
x	arbitrary function	---
$\overline{\quad}$	mean component of a quantity	---

Abstract

This study investigated the effect of multiple cylinders positioned within 6 diameters on the formation of von Karman vortex streets. This research effort used a water tunnel and a modified free jet to create desired flow conditions. Both flow visualization and hot film data were obtained under various conditions.

Circular cylinders were used as models for the creation of the vortex street. A water table was modified into a water tunnel which was run at various flow velocities to produce flow conditions at $Re_D \leq 1 \times 10^4$. Shadowgraph-type photos were taken of the water flow field. A free jet was run at various flow velocities to produce flow conditions at a higher Re_D. A diverging dead-wake pattern was created by .794 cm diameter rods placed at the exit of a 1 cm by 10 cm free jet at M = .1 and .6. Classical vortex streets were created using the same size cylinder and a 5 cm by 5 cm free jet nozzle with an attached channel. Both schlieren photographs and hot film measurements were taken of the flow fields at $Re_D = 1.1 \times 10^5$ and 1.88×10^4 respectively.

The water tunnel results indicate the formation of the von Karman vortex street has no dependence on either the absence or presence of other cylinders. The free jet data confirmed the water tunnel results and showed that dependence

of the von Karman vortex street in the gas flow facility used in this study was due to jet conditioning and ultimately could be produced for this size cylinder in a duct (i.e. in closed tunnel surroundings). Diverging dead-wake patterns were formed when no duct was present. Statistical hot film data taken at M = .1 substantiated these results.

EFFECTS OF MULTIPLE CYLINDERS ON THE FORMATION OF VON KÁRMÁN VORTEX STREETS

I. Introduction

Flow past a circular cylinder has been an extensively investigated phenomenon. In particular, the von Kármán vortex street has been the focus of many experimentalists as well as theoreticians (Refs 1,2,3, and 4). The formation and shedding of these vortices are just two of the characteristics that have been reported. The eddy size and spacing generated by the cylinder forms a wake pattern that seems to be virtually predictable. The predictability of the shedding frequency and the estimation of eddy size are qualities that contribute to the study of turbulence. Thus, it appears that the creation of a von Kármán vortex street could be ideal for generating a well defined turbulent flow field. This concept was initiated during a study investigating the effects of turbulence on the degradation of a laser beam (Ref 5). By using a free jet and a row of two or more cylinders, several streams of compressible vortices were created. However, no well defined vortex street was evident.

The ability to create one or more von Kármán vortex streets can be a valuable asset in the study of turbulence and its effect on laser beam intensity. Since this was not

entirely successful (Ref 5), it has been suggested that there may be some dependency of the formation of multiple vortex streets on the geometric location of the cylinders generating the turbulence (Ref 6). The initial purpose of this study was to determine the dependency of cylinder location on the formation of a von Kármán vortex street so that a "good" turbulence pattern could be created for future laser work.

From this background, the following objectives were developed for this research:

1. Simulate, using the water table, the flow field produced by multiple cylinders positioned at the exit of the free jet.
2. Create a characteristic vortex street in the water medium by varying the cylinders' locations relative to each other.
3. Demonstrate the dependency of the vortex street formation on cylinder location with the free jet using schlieren photographs of the flow fields.
4. Produce statistical data of the flow fields using hot film measurements.

The balance of the report focuses on the means by which the objectives were achieved and the results of the research. Section II discusses the theory and approach taken. Sections III and IV describe the test apparatus and procedure used. Section V discusses the results and Section VI the conclusions. The final section contains recommendations for further investigation.

II. Theory and Approach

The well documented theory of vortex streets was applied to the free jet (Refs 7 and 8) and to the water table (Ref 9).

Periodic Flow Field Creation

The phenomenon of the von Kármán vortex streets has been studied over a large range of Reynolds numbers based on cylinder diameter, Re_D. Schlichting presents the relationship between Strouhal number and Re_D for which vortex streets appear (Ref 10: 31-33). This relationship is summarized in Figure 1.

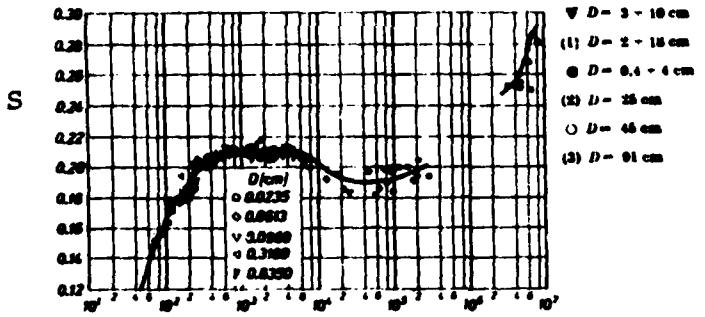

Figure 1. Strouhal Number as a Function of Reynolds Number (Ref 10: 32)

Because of the extensive reporting of the phenomenon in the literature, the difficulty in forming vortex streets for multiple cylinders was attributed to interference effects between cylinders (Ref 6) and possible compressibility ef-

fects. The compressibility effect, however, seemed less likely since others (Refs 2 and 10) have demonstrated vortex streets in a compressible domain of near identical Mach and Reynolds number as those of Reference 5. This is shown in Figure 2. If the effect is not compressibility related, the water tunnel seemed well suited to investigate interference effects, as these tunnels have been shown to similarly demonstrate vortex street phenomena (see Fig. 3), as long as the extrapolation of the findings are kept within the acceptable Re_D limits.

The formation of the vortex street pattern has been categorized by Roshko (Ref 4) as having a stable range, $40 < Re_D < 150$, a transition range, $150 < Re_D < 300$, and an irregular range, $300 < Re_D < 10{,}000+$. Below $Re_D = 40$, two bound, symmetric vortices remain attached behind the cylinder. At about $Re_D = 40$ the vortices begin to oscillate and start shedding alternately from the cylinder to form a street pattern. As the Re_D increases up to approximately 150, stable vortex shedding occurs and has a definite periodic pattern predictable by the Strouhal number

$$S = \frac{fD}{v} \qquad (1)$$

where f is the frequency of the shed vortices, D is the diameter of the cylinder, and v is the flow velocity. The transition range of the vortex pattern is characterized by intermittent laminar and turbulent boundary layer stability.

Figure 2. Compressible Vortex Street, M = .556, $Re_D = 2.7 \times 10^5$ (Ref 2: 109)

Figure 3. Vortex Street in Water, Re_D = 105 (Ref 11: 57)

The actual formation of the vortices in the range has laminar to turbulent transition occurring in the boundary layer as the shear layer separates from the cylinder. The irregular range has an earlier transition taking place in the shear layer giving way to the shedding of vortices containing completely turbulent fluid as depicted in Figure 4. Thus, the large range over which the irregular wakes appear (cf. Fig. 1) is to be avoided in any experimental study creating von Kármán vortex street data.

The lower Re_D range of the vortex street can be created on the water table, and in the present case, the maximum flow rate provided by the water pump is the limiting criterion restricting the highest Re_D that may be obtained. Since the maximum flow rate possible in the present study was 72 gallons per minute, the Re_D of the water table was limited to 1×10^4 for reasonable cylinder diameters. For this Re_D, the hydraulic analogy applies in that changes in water depth are related to changes in air pressure in the gas flow analogy (Ref 9). Thus, it became necessary to modify the water table configuration into a water tunnel (see Section III), in order to provide a more realistic pressure field. Results obtained in the water tunnel were then compared to the higher Re_D range of results achieved by use of the free jet. The diverging dead wake pattern of Reference 5 was obtained at $Re_D = 1.1 \times 10^5$. Therefore, the jet experiments were performed from near the Re_D of the water tunnel up to 10^5.

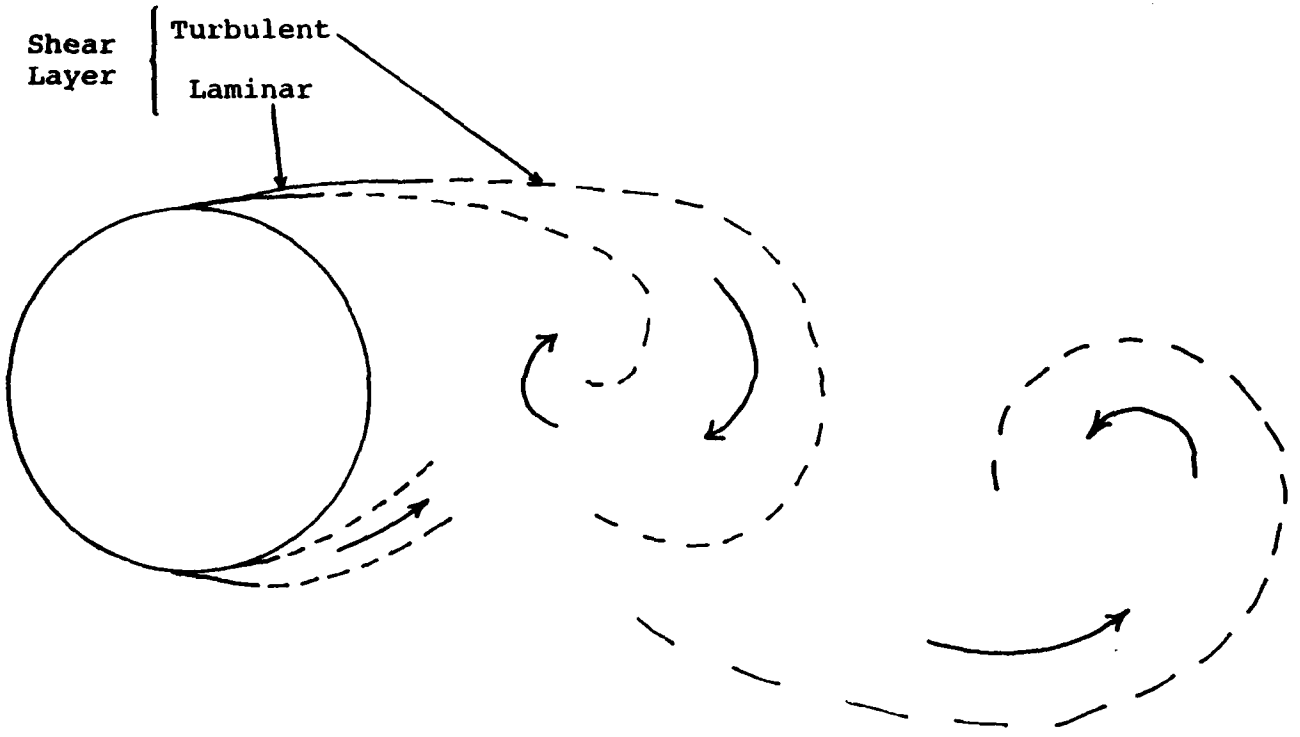

Figure 4. Von Kármán Vortex Street, Re_D > 40 (After Refs 4: 816 and 2: 113)

The vortex streets for both the water tunnel and the modified free jet were created by placing circular cylinders in the center of the flow field. The water tunnel cylinders were oriented perpendicular to the table surface. The ducted free jet cylinders were mounted on a frame which secured the rods to the jet exit plane normal to the flow. Both devices then were easily capable of providing the required flow conditions for this research effort.

Visualization of Flow Field Structure

"Streaklines" in the water flow field were made visible by use of a colored dye injected into the flow. The requirement of the dye injection system is that it be nonintrusive. The smaller the amount of upstream disturbances, the more accurate the dye will be in recording the true flow field. Once the "streaklines" are made satisfactorily visible, standard photographic techniques could then be used to record pertinent data.

Toepler-schlieren photography was used to record the density gradients in the flow field of the free jet. In general, as a nearly collimated light source passes through the density gradients in the flow field, the light is refracted and consequently when refocused, light and dark areas appear. Since the frequencies of the shed vortices in the free jet flow field were anticipated to be on the order of 5 kHz (see Eq. 1), a spark lamp and high speed film were

necessary to capture the nature of the flow field satisfactorily (Ref 5: 3,4,10). Toepler-schlieren photography was also used for flow field visualization of incompressible flow. The density gradients needed for the accomplishment of this technique were provided by helium injection into the flow field (Ref 12). Since helium is less dense than air, gradients form as the helium is carried and dissipated downstream. Thus, a free jet flow at Mach number, M = .1 could be made visible by injecting helium gas into the airstream at the desired location.

Flow Field Measurement

A single hot film probe was placed in the flow field downstream of the cylinders and oriented normal to the flow and parallel to the cylinders. The probe was capable of traversing across and downstream of the jet exit to collect data at any point desired in the flow field. The signal generated by the hot film anemometer was then analyzed for periodicity by the use of an on-line autocorrelator and frequency spectrum display.

An autocorrelation computation determines the periodic data otherwise masked by varying random signals. An estimate for the autocorrelation of a signal at time t and $t + \Delta t$ is found by taking the product of the two signals and then averaging a large number of these products taken over a total sample time, T. The average product will approach the

true autocorrelation function, $R_c(\Delta t)$, as the sample time, T, becomes very large, i.e.

$$R_c(\Delta t) = \lim_{T \to \infty} \frac{1}{T} \int_0^T x(t)\, x(t+\Delta t)\, dt \qquad (2)$$

Example signals appear in Figure 5 with their respective autocorrelation functions in Figure 6 (Ref 13: 17-21).

The power spectral density function as determined by the frequency spectrum display describes the general frequency composition of the input signal. A property of the power spectral density function, G(f), is that it is related to the autocorrelation function by a Fourier Transform

$$G(f) = 4 \int_0^\infty R_c(\Delta t) \cos 2\pi f\, \Delta t\, d(\Delta t) \qquad (3)$$

The power spectral density plots of the signal in Figure 6 are shown in Figure 7. Note that the arrow at f_o denotes an infinite spike at the frequency of the sine wave (Ref 13: 22-25). Thus, the anemometer, correlator, and spectrum display provided information about the periodic nature of the flow in comparison to the generalized information provided by the schlieren photographs.

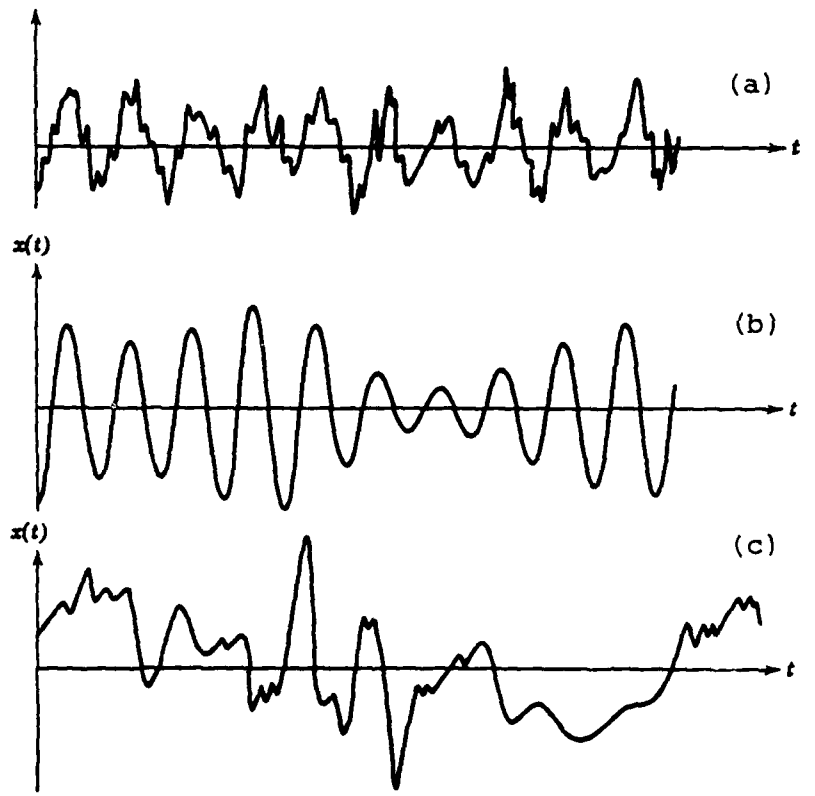

Figure 5. Turbulence Signals. (a) Sine Wave Plus Random Noise. (b) Narrow-Band Random Noise. (c) Wide-Band Random Noise. (Ref 13: 17)

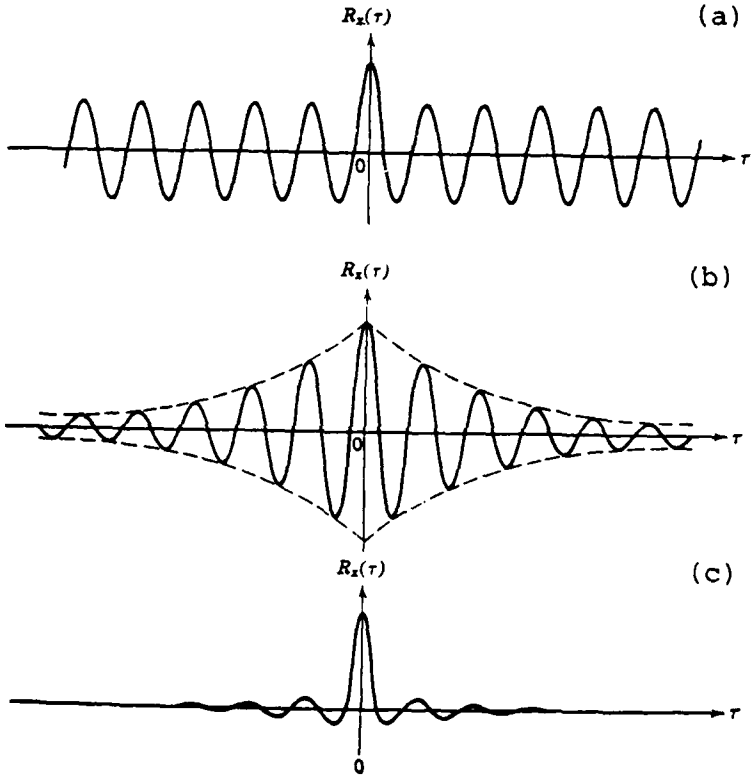

Figure 6. Autocorrelation Functions of Turbulent Signals. (a) Sine Wave Plus Random Noise. (b) Narrow-Band Random Noise. (c) Wide-Band Random Noise. (Ref 13: 21)

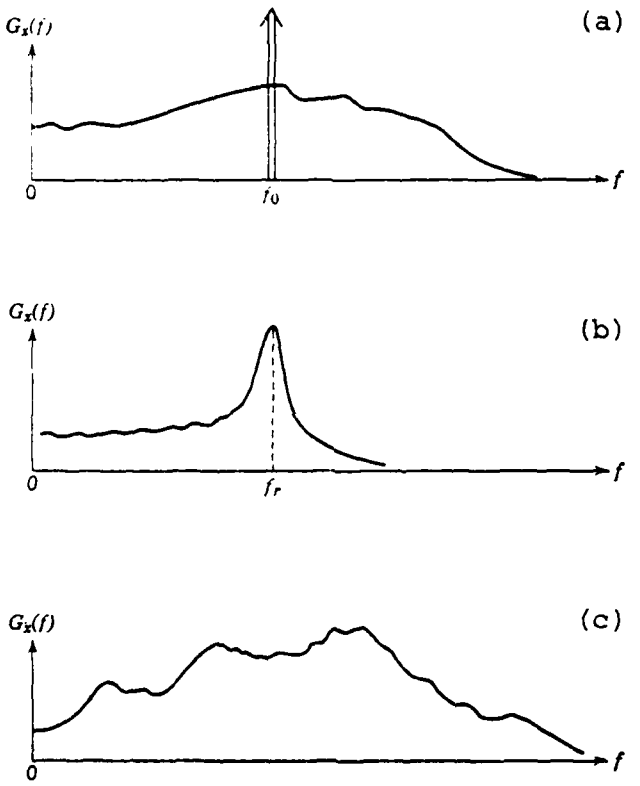

Figure 7. Power Spectral Density Plots. (a) Sine Wave Plus Random Noise. (b) Narrow-Band Random Noise. (c) Wind-Band Random Noise. (Ref 13: 24)

III. Experimental Apparatus

The test apparatus consisted of a water table modified as a water tunnel with several cylinders of various diameters, a dye injection system with photographic equipment for flow visualization, and a free jet with various cylinders and modifications, an electronic measurement system to analyze the flow field, and a schlieren photography system for flow visualization. Since two completely separate test devices were used, the modified water table and its associated systems will be described before the free jet and its systems.

Water Table

The water table has been used extensively as a flow visualization tool for a large variety of flow phenomena. Many of the recent uses of this device took advantage of the hydraulic analogy to visualize specific flow characteristics (Refs 9,14, and 15). In this study however, dye injection was used as the primary means of flow visualization to investigate the lower Re_D range.

Since the hydraulic analogy is not applicable to the desired flow field, the water table was modified and used as a water tunnel. The dimensions and characteristics of the modified water table essentially remained the same as in previous studies (see above). One modification made was the water pump. For this study the 1/3 horsepower pump was re-

placed with a 3 horsepower centrifugal pump. The second modification made was that a clear plexiglass sheet (1.23 m x .85 m x .32 cm) was positioned on top of the wood blocks and secured with weights. Thus, the flow was subjected to a uniform tunnel pressure field for the length of the plexiglass.

Aluminum cylinders of 2.45 cm, 5.08 cm, and 7.62 cm diameters were used as models to create the periodic flow field. The wood blocks used to restrict the width of the flow field were 4.56 cm thick. Therefore, for consistency of the tunnel depth, the cylinders were also 4.57 cm tall. The water tunnel then had a depth of 4.57 cm and a length of 1.23 m. The width of the tunnel was varied to create different flow rates and thus different Re_D.

The dye injection system consisted of a hollow metal 1.83 mm diameter tube approximately 43.2 cm long. One end of the metal tube was positioned through a plexiglass block so that the tube could be secured to the water tunnel structure. Flexible tygon tubing was attached to the end of the metal tube for feeding of the dye from the plastic syringe (Fig. 8). Condensed milk was used as the fluid injected into the flow. This relatively dense dye allowed better visualization for the higher flow rates. Food coloring was added to the dye for easy visualization.

To ease the photographic problem, an overhead type projection device was used. The base or lighted portion of the

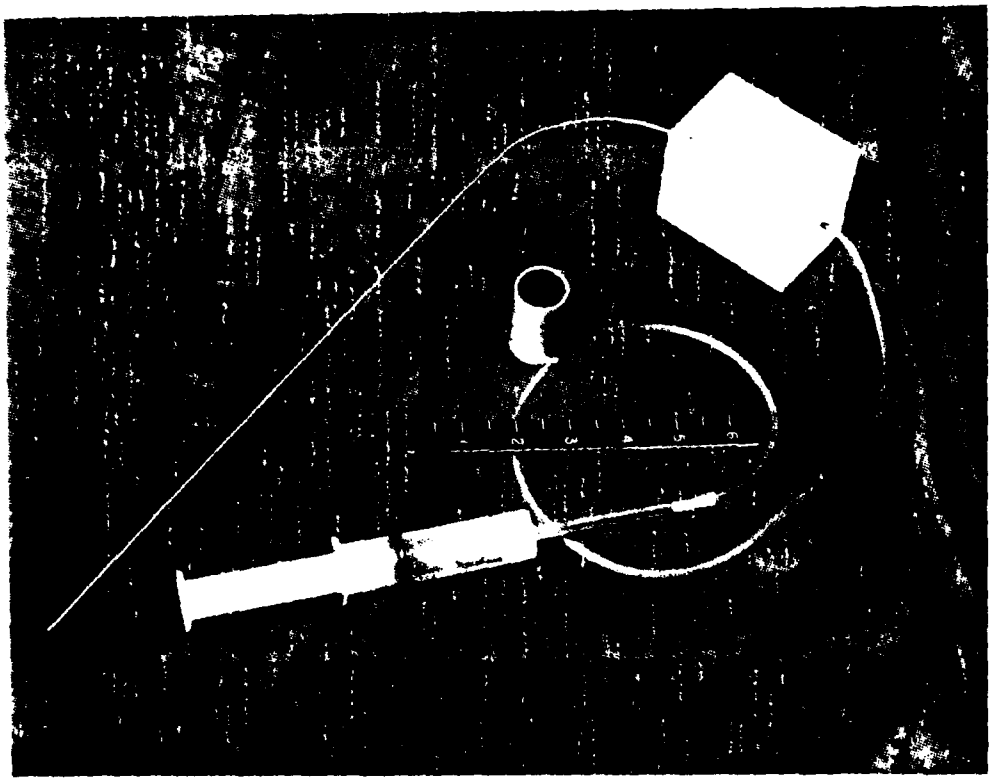

Figure 8. Flow Injection Device and Circular Cylinder Model.

projector was positioned below the glass table surface as close as possible to the underside of the glass. The overhead lens and mirror were secured to a crossmember which was attached to the sides of the water table structure. The lens fixture could be adjusted for focusing of the test section image (Fig. 9). White poster board was taped on a nearby wall so that the lens projected a large clear image of the center of the water tunnel area. This overhead projection system allowed shadowgraph type images to be projected for water table operation (although the mechanism for producing the images was the presence of the dye rather than the water surface in the case of a true shadowgraph).

Free Jet

The capabilities of the AFIT free jet facility have been thoroughly studied and documented (Refs 7 and 8). Since Weston obtained his unusual results with this facility, it was obvious that this study should also employ the same free jet. The cylinders used for the periodic flow field were the same diameter as those used by Weston (.794 cm), as well as the mounting system and jet configuration (Ref 5: 13-15).

Because several minor modifications were made to the cylinders and the free jet nozzle, the reader is referred to Appendix A for a detailed listing of all the modifications and their effects while details of the more significant changes are described here. Hollow 1.905 cm long tubes were used as spacers separating the frame upon which the tested

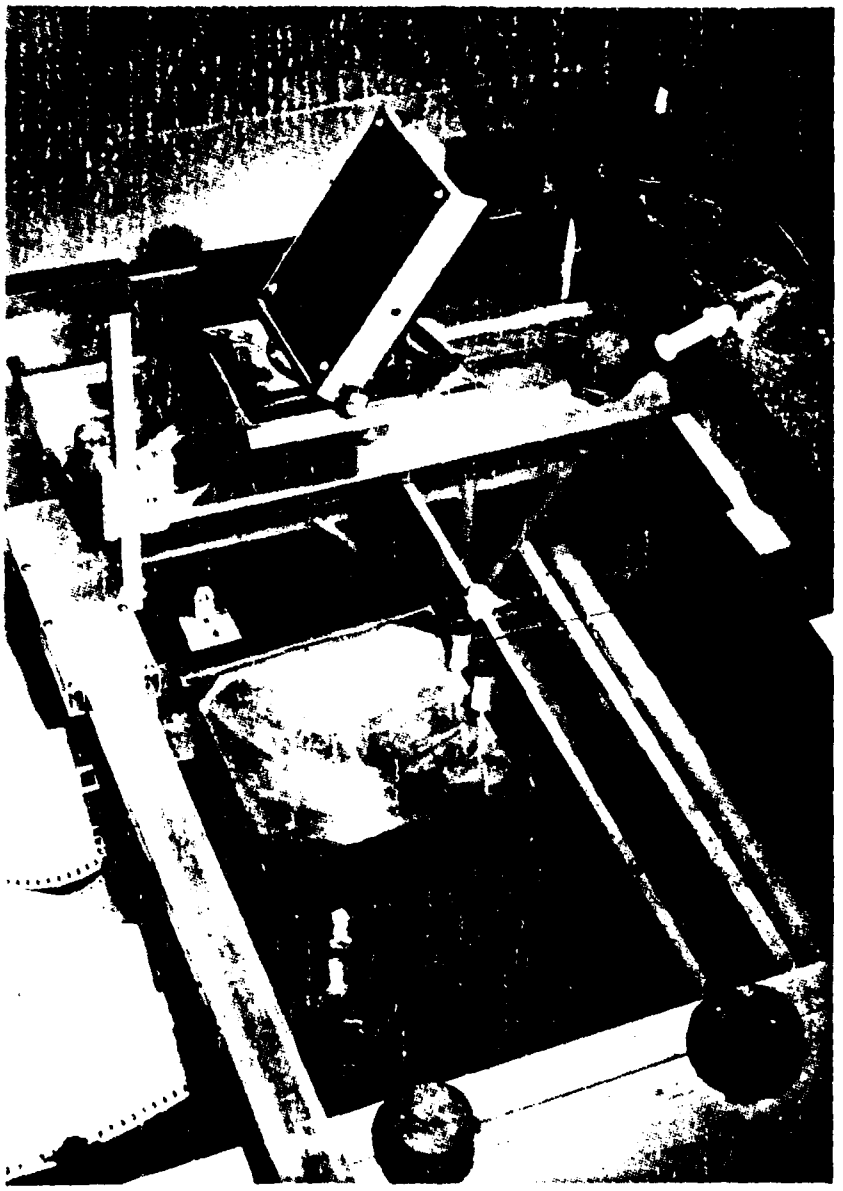

Figure 9. Water Tunnel and Overhead Projection Arrangement.

cylinder was attached and the mounting block that was secured to the jet nozzle as shown in Figure 10. A cylinder was adapted such that a secondary gas supply could be passed through a tube into the cylinder and then injected out into the airflow. This cylinder allowed a pressurized helium supply to be attached to it without affecting the characteristics of the flow field. As shown in Figure 11 the cylinder contained 5 exit ports each with a diameter of 1.59 mm. A jet nozzle with a 5 cm by 5 cm exit plane was also fabricated such that it was compatible to the free jet and could be interchanged with the existing 1 cm by 10 cm nozzle. The square nozzle had a similar block welded to it such that plates holding cylinders could be fastened in the same manner as with the rectangular nozzle. A square channel 12.7 cm long with an inside dimension of 5 cm by 5 cm was made so that it could be attached to the cylinder frame. The channel was void of any lip or step which could affect the flow field as it passed into and through the channel. Also the two sides perpendicular to the cylinder were made of glass to allow schlieren photographs to be made of the flow within. The channel could be removed or attached without affecting the cylinder or its position with respect to the jet exit. These cylinder and nozzle modifications were used systematically in a manner that allowed sufficient data recording to explore the effects independent of other influencing parameters.

Figure 10. 1.905 cm Spacers, Free Jet Rectangular Nozzle, and Hellium Injection Cylinder Arrangement.

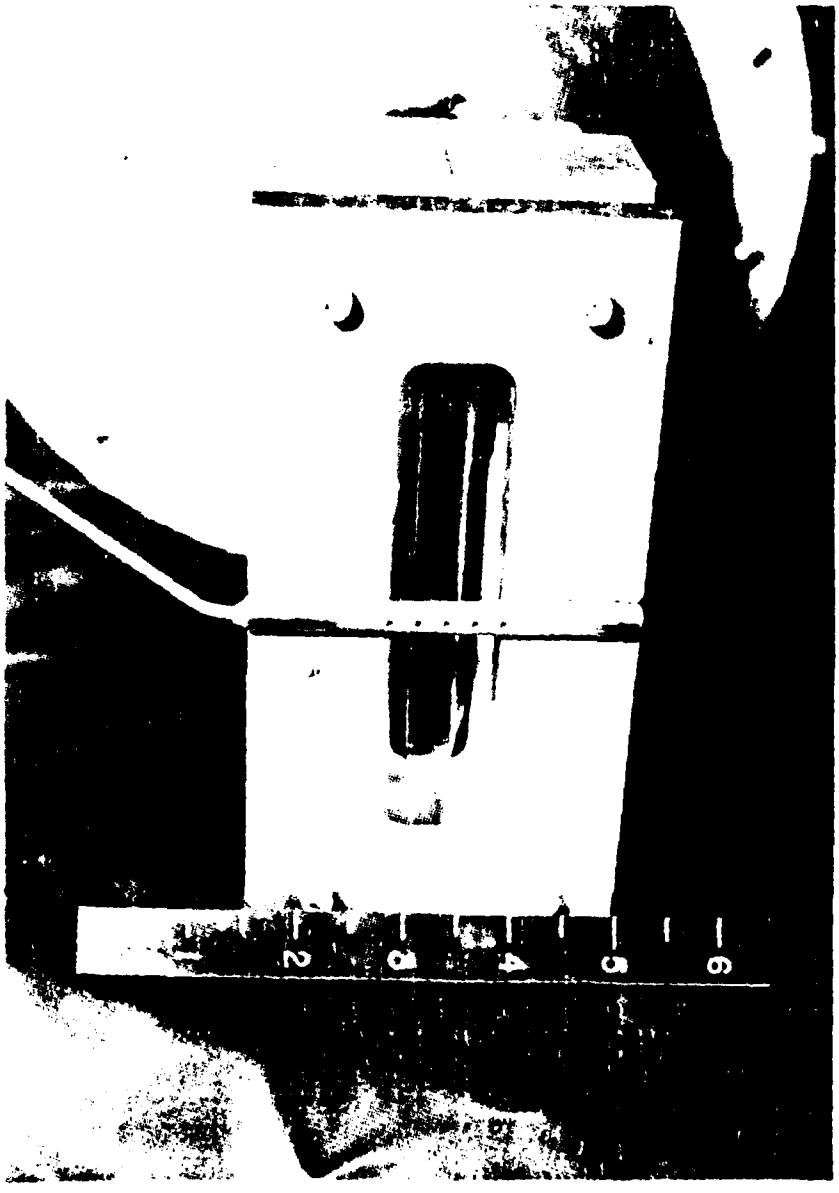

Figure 11. Helium Injection Cylinder Attached to the Rectangular Nozzle.

The equipment used for the Toepler-schlieren system is depicted in Figure 12. Since the system is the same as that used in a previous study, no further description of the devices is necessary (Ref 5: 21-25).

The hot film anemometer is an accepted tool used in turbulence studies and needs no theoretical description. It was used to measure velocity fluctuations for the nearly incompressible flow field created by the free jet. The entire electrical system is shown in Figure 13. A single element Thermo-Systems, Inc. (TSI) 1214-20 .005 cm diameter hot film sensor was oriented parallel to the cylinder located at the jet exit. The hot film sensor was attached to an elbow mount which was secured to the L shaped arm of a Gaertner Scientific Co. cathetometer. This allowed the hot film to be positioned securely anywhere in the flow field within $\pm$ .005 cm, and it allowed the cathetometer to be located away from the flow field. The hot film was operated at a constant temperature of 250°C and connected to a TSI Model 1050 anemometer. The mean and fluctuating voltages from the anemometer were measured by a Hewlett-Packard (HP) 34740A digital voltmeter and an HP 3400A RMS voltmeter respectively. The same anemometer signal was also displayed on a Tektronic 465M oscilloscope to obtain a qualitative picture of the turbulence level. The anemometer signal was also received by an HP 3721A correlator. Set in the autocorrelation mode, the turbulent signal was then correlated

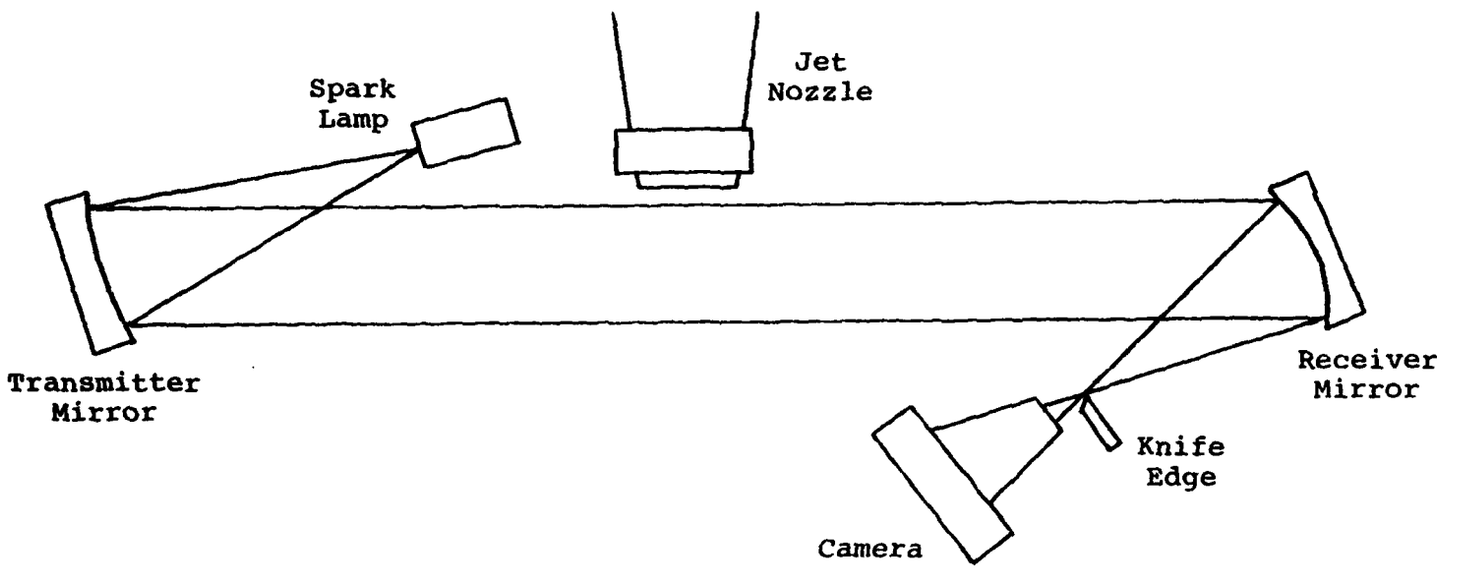

Figure 12. Schlieren Photography System Arrangement.

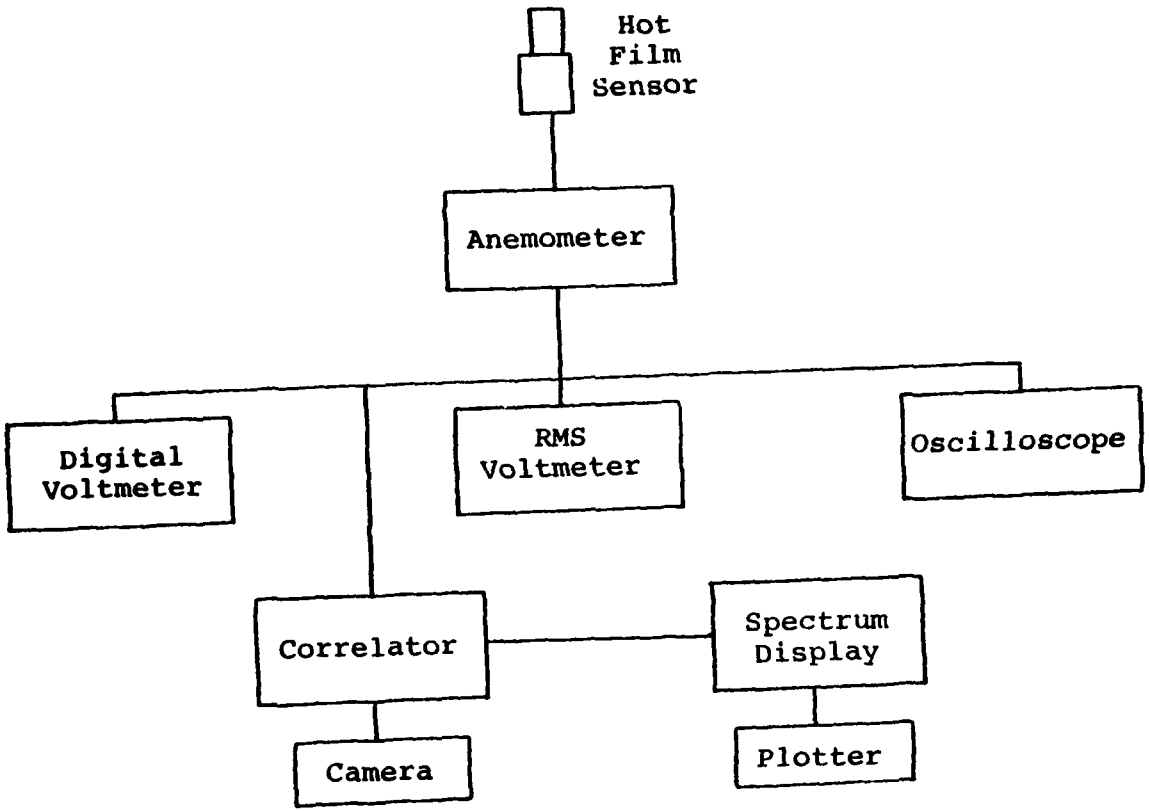

Figure 13. Hot Film Statistical Measurement Arrangement.

with itself and the resulting function displayed on its cathode ray tube (CRT). A poloroid camera using type 42 ASA 300 film was mounted on the HP 3721A so that data could be recorded. The correlation signal was then passed to the HP 3720A spectrum display. The spectrum display processed the correlation data to form a power spectral density plot displayed on its CRT. The functions displayed on this CRT were recorded on an HP 7045B plotter. This electrical system was a modified version of one used in an earlier study (Ref 5: 17-19).

IV. Experimental Procedure

Prior to any data gathering, equipment calibration was performed, flow measuring devices were carefully aligned, and trial runs were made. This allowed check-out and familiarization of the measurement and data collection equipment as well as elimination of possible procedural errors.

Water Tunnel

In preparing the water tunnel for an experimental run, the test section was made by placing wooden blocks on the table surface to form a channel. The width of the channel coupled with the volume flow rate of the pump determined the flow velocity at the test section and hence the Re_D. The test cylinders could then be positioned as desired in the channel. The dye injection tube was placed near the upstream portion of the cylinders to preclude early dissipation of the dye. Once the test section was positioned as desired, the plexiglass sheet was positioned over the test section supported by the wooden channel blocks. Weights were placed over top of the plexiglass at its perimeter and on the wood blocks. The front dam was lowered to the top of the plexiglass and the blocks to prevent water flowing on top of the test section. Tape was also used to help prevent water from seeping onto the top of the plexiglass (cf. Fig. 9).

The resevoir tanks were filled from the local water

supply. The usual water table operation required approximately 2 to 4 cm of water depth above the plane of the test section. In the modified water tunnel configuration, however, 4.57 cm of water depth was needed. Several minutes of water pump operation were needed before the water flow through the test section reached steady flow conditions. The amount of back pressure needed for tunnel operation was controlled by adjusting the weir height. The flow rate was regulated by the valve controlling the amount of flow to the pump. For substantial changes in flow rate both the channel width and the regulating valve were altered. For each Re_D tested the cylinders were varied from 2 to 6 diameters lateral separation distance. The upstream position of one cylinder in reference to the second was also varied from 0 to 2 diameters offset. In this way the variation of cylinder location both in the upstream direction and the crossflow direction was investigated for several Re_D.

For each data point at a specific Re_D and cylinder location the flow field was tested by injecting the dye into the field slightly upstream of one of the cylinders. The dye was previously mixed from condensed milk and food coloring for an acceptable color and consistency as determined from earlier trial runs. The amount of dye injected into the flow field was controlled by the amount of pressure applied to the syringe. Data was recorded as necessary by photographing the flow image projected on the wall.

Free Jet Schlieren Photography

The setup and alignment procedures which are critical for obtaining high quality and high resolution photos were closely followed as described in previous research (Ref 5: 31).

The temperature and pressure of the air in the calming chamber of the free jet were assumed to be stagnation or total conditions since the velocity in this region was negligible. Thus the isentropic flow relationship

$$\bar{P}_o = \bar{P}_e \left[1 - \frac{\bar{v}^2}{RT_o} \left(\frac{K-1}{2K} \right) \right]^{-\left(\frac{K}{K-1} \right)} \qquad (4)$$

may be applied to give the required stagnation pressure in the free jet for the desired average velocity for M = .6. Fluctuations in air pressure occurred at these operating conditions which required close monitoring of the stagnation pressure. The same procedure to determine stagnation pressure was followed for M = .1 flow conditions. The helium injection needed for incompressible flow visualization was supplied from a pressurized tank. Caution was used to insure the helium line pressure did not exceed 5 kg/cm^2 to assure non-interference with the main flow field. Schlieren photographs were then used to record the flow field characteristics.

Free Jet Velocity Fluctuation Measurement

The single hot film sensor was first calibrated in an apparatus similar to the TSI 1125 calibrator. General cali-

bration instructions were followed according to the TSI manual (Ref 16: 2.2-2.9). A voltage-versus-velocity curve was then made for the anticipated operating regime of the hot film sensor. The sensor was then installed in the elbow support and fairing as depicted in Figure 14. A meticulous alignment procedure was then followed using theodolites positioned normal to the flow stream at the jet exit and far downstream in the center of the flow field. This allowed the probe to be aligned normal to the flow and parallel to the cylinders in all three dimensions as described in Reference 5. Once the sensor was positioned and aligned at the initial data point location, cathetometer readings were recorded as the reference location. This location was the basis for further data point positioning. Each time the sensor was replaced, alignment and reference positioning were performed again.

Since the hot film measurements were obtained at M = .1, the free jet was controlled by regulating the stagnation pressure as described above using Eq. 4. For the single cylinder with and without the 1.905 cm spacers, data points were taken from the flow field centerline outward to the edge of the turbulence. Lateral positioning for data was at one-half cylinder diameter increments. Downstream positioning was referenced initially at two diameters and continued downstream at one diameter intervals to five diameters. For the single cylinder with the channel attachment, data was taken

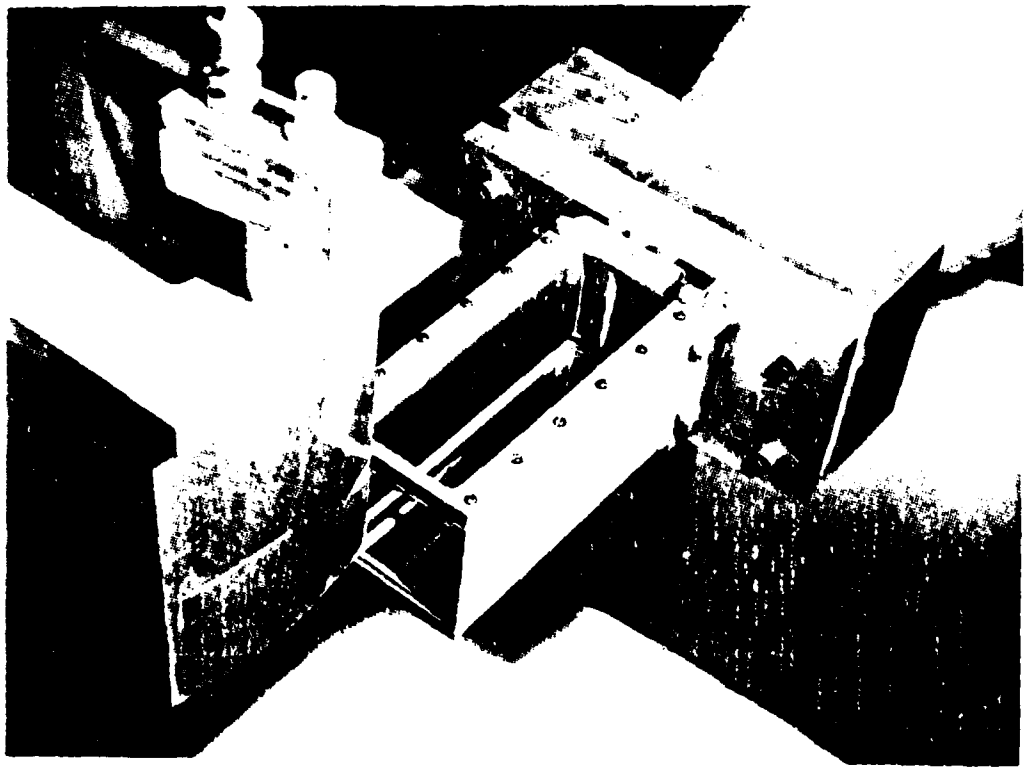

Figure 14. Hot Film Positioned in the Channel Flow Field of the 5 cm by 5 cm Nozzle.

at 9 1/2 and 12 diameters downstream due to fairing and channel interference. The flow field within the channel was probed laterally at one-half diameter increments initiated at the centerline. The channel width permitted 11 data points to be taken for each downstream location. At each data point velocity measurements, autocorrelation information, and power spectral density plots were recorded.

V. Results and Discussion of Results

Von Kármán vortex streets were successfully created in both the water tunnel and the modified free jet flow fields. The periodic flow fields were studied to determine if the vortex streets would change structure when a second cylinder was positioned nearby. Flow field statistical measurements were recorded for single cylinder flow fields from the free jet. Schlieren photographs of these flow fields coupled with the hot film measurements gave a firm basis for study of the vortex shedding phenomenon.

Water Flow Field

No problems were encountered in creating a von Kármán vortex street throughout the range of Re_D tested in the water tunnel. As the flow velocity increased, however, increased turbulence partially masked the vortex street making it difficult to observe and photograph. As the cylinders were positioned from 2 to 6 diameters apart laterally and 0 to 2 diameters axially, the characteristic vortex street appeared behind each cylinder for each separate cylinder location. There appeared to be no change in the periodicity or the structure of the vortices. Because there was only one dye port, the phase relationship between the two vortex streets could not be observed. Since flow visualization was the objective of the water tunnel study, no exact flow measurement

data was taken. A representative water flow photograph is shown in Figure 15.

The diverging dead wake pattern encountered by Weston using the free jet and two cylinders (Ref 5: 40) could not be duplicated in the water tunnel. It was suggested that the flow field created on the free jet ($Re_D = 1.1 \times 10^5$) was more a result of the Re_D being close to the unstable range ($Re_D > 3 \times 10^5$, from Fig. 1), combined with the close proximity of a second cylinder (Ref 15). Since the water tunnel produced a maximum Re_D of approximately 1×10^4, the facility could not further substantiate this hypothesis.

Free Jet Flow Field

Three basic nozzle/cylinder configurations were investigated using the free jet at Mach numbers of .1 and .6. Each of these configurations was further broken down into sub-configurations as indicated in Table I.

The first configuration was identical to that described by Weston (Ref 5: 15-17). The jet exit was 1 cm by 10 cm, and had a flange welded .873 cm from the exit plane for attaching the cylinder-holder bracket (see Fig. 10). The bracket holding the cylinders was mounted such that the cylinders were flush against the jet exit. Since the attachment bracket was larger than the jet exit, a recirculation cavity in the shape of a rectangular torus was created when the mounting bracket was in place. The first set of sub-configurations differed in the separation distances and number

Figure 15. Von Kármán Vortex Street with Turbulence in the Water Tunnel, $Re_D = 9.95 \times 10^2$

TABLE I

NOZZLE/CYLINDER MODIFICATIONS

Configuration Number	Nozzle Size	Modification	Centerline Cylinder Spacing
1	1 cm x 10 cm	Nozzle/Cylinder Spacers of Length (cf. Fig. 10)	8D,6D,4D (cf. Fig. 16)
a.		1.27 cm	8D,6D,4D
b.		1.59 cm	8D,6D,4D
c.		1.905 cm	8D,6D,4D
d.		2.54 cm	8D,6D,4D
e.		3.175 cm	8D,6D,4D
2	5 cm x 5 cm		
a.		Normal Bracket Mounting (Cylinder-Nozzle Separation = .953 cm)	
b.		Reversed Bracket Mounting (Cylinder-Nozzle Separation = 0 cm)	
3	5 cm x 5 cm	Duct Attached (cf. Fig. 14)	
a.		One Cylinder	
b.		Two Cylinder	3D

of cylinders. The cylinder size used was that of the number 2 grid from Weston's study (Ref 5: 17), which had a cylinder diameter of .794 cm. A single cylinder configuration was run as well as a two cylinder configuration with various spacings as described in Table I. At a Mach number of .6 all arrangements gave identical flow patterns when observed using schlieren photography. An example photograph is shown in Figure 16. Each flow pattern was identical in all details to that described by Weston (Ref 5: 39-43). Contrary to that which had been postulated, there appeared to be no interference effect and no dependence on cylinder spacing. The flow from this series of runs may best be described as a diverging, dead wake eminating from behind the cylinders. This wake was bordered by an unstable shear layer that showed some periodicity, but clearly lacked any organized vortex street arrangement. The flow also exhibited separation from the cylinders at a point upstream from the separation point expected from descriptions of flow around cylinders reported in the literature (Ref 6: 170-173, 215-216). The configurations were rerun at a Mach number of .1 and the flow observed using schlieren photography by bleeding helium into the wake, as previously described. The character of the wake appeared to be unaffected by the Mach number change (see Fig. 17).

The first configuration was slightly modified for an additional series of runs. Because the original configuration gave rise to a recirculation cavity, this cavity was identified as a possible cause for the diverging dead wake

Figure 16. Schlieren Photograph of Wake Pattern for 4 Diameters Separation at M = .6.

Figure 17. Schlieren Photograph of Helium Injection Cylinder Flow at M = .1 .

pattern. To eliminate this cavity, spacers of varying size (Table I) were added. This modification allowed a purge flow to be maintained by jet entrainment. Crude measurements using flexible vanes indicated that the purge flow was sizable but much smaller than the main flow. This modification showed an effect on the flow pattern as observed in the schlieren photographs at both Mach numbers, .6 and .1 (the latter made observable by bleeding helium into the wake). The divergence angle of the wake was much smaller from the previous half angle of 21° for the nonspacer configurations to a new half angle of 12° (see Fig. 18). The optimum gap space was found to be 1.905 cm. The flow quality, however, was much the same as that of the first configuration, and did not exhibit a vortex street in the classical sense. Again, no interaction effects were exhibited.

Since it was judged that the flow fields at both Mach numbers were virtually identical, the lower Mach number was used to further characterize the flow in order to avoid the complications of probe resonances biasing the signals as encountered by Weston at the higher speed (Ref 5: 51-52). The best of the diverging dead wake patterns from the first configuration, was rerun at a Mach number of .1 and the flow field characterized using the hot film anemometer at the flow field locations shown in Table II. A representative sample of these is shown in Figure 19. These power spectral density plots indicate low frequency wideband turbulence

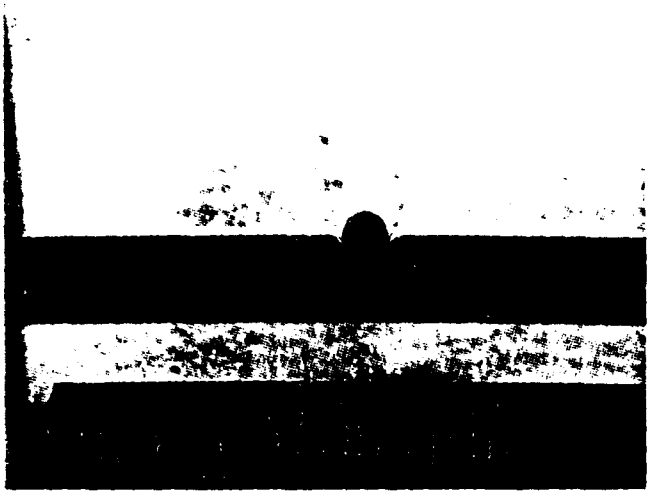

(a)

(b)

Figure 18. Schlieren Photographs Comparing Flow Fields (a) With and (b) Without Spacers, M = .6 .

TABLE II

HOT FILM MEASUREMENT TEST POINTS FOR

CYLINDER WITH SPACERS

Test Point	Centerline Axial Location	Centerline Lateral Location
1	2D	0D
2	2D	1/2D
3	2D	1D
4	3D	0D
5	3D	1/2D
6	3D	1D
7	3D	1 1/2D
8	4D	0D
9	4D	1/2D
10	4D	1D
11	4D	1 1/2D
12	4D	2D
13	5D	0D
14	5D	1/2D
15	5D	1D
16	5D	1 1/2D
17	5D	2D

(see Fig. 7). Appendix B contains the complete data set.

The second configuration was a modified nozzle exit of dimension 5 cm by 5 cm. This configuration change was designed to alter the length-to-diameter aspect ratio of that part of the cylinder exposed to the flow in order to investigate the aspect ratio dependence of the diverging dead wake pattern. This configuration was studied with single and

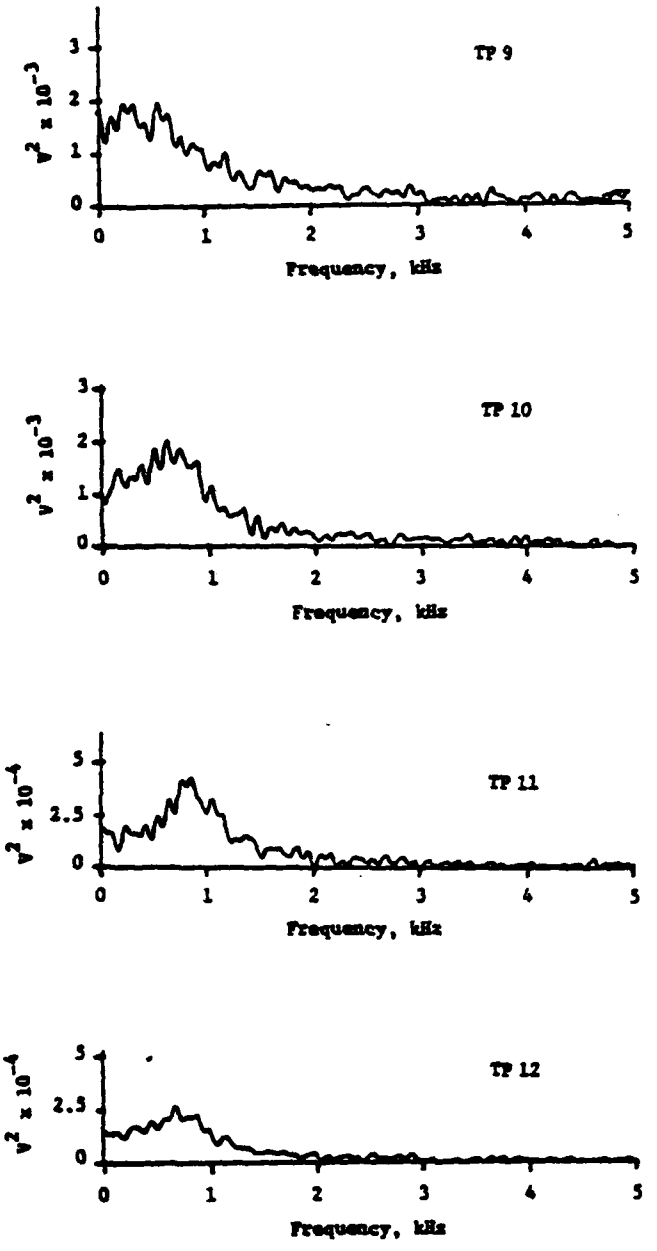

Figure 19. Power Spectral Density Plots of Single Cylinder Wake Pattern Using Spacers, M = .1 (TP 9 - TP 12).

double cylinders and with and without spacers in the same manner as the first configuration. The flow pattern's interference effects, and spacer effect appeared to remain identical to that of the first series with the smaller aspect ratio. Thus the diverging dead wake pattern appeared to be unaffected by aspect ratio. Schlieren photographs were again used to judge the quality of the flow as in the previous cases. A representative photo is shown in Figure 20.

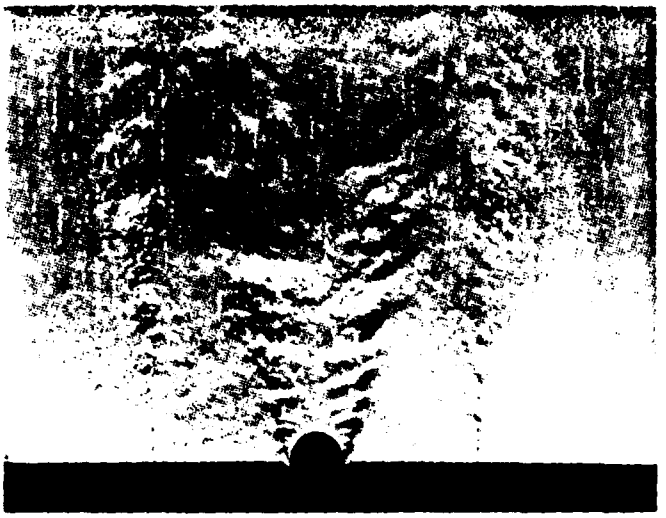

Figure 20. Schlieren Photograph of Single Cylinder Flow Field Using the Square Nozzle and 1.27 cm Spacers, M = .6 .

In an attempt to mount the cylinders closer to the jet exit, one run using the 5 cm by 5 cm nozzle was made with the cylinder mounting bracket reversed. Because of the bracket dimensions, the bracket formed a closed channel approximately 1.1 cm long behind the cylinder. Schlieren photographs, made at a flow Mach number of .6, showed the first signs of a

partially organized vortex street (see Fig. 21).

Figure 21. Schlieren Photograph of Single Cylinder Flow Field Using the Square Nozzle and the Reversed Bracket Mounting, M = .6 .

In order to check the dependence of the quality of the vortex street on the presence of an enclosed channel, a third configuration was designed and tested.

The third and final configuration involved flush mounting the cylinders of the large aspect ratio configuration and adding an enclosing duct 12.7 cm long as described earlier. This configuration change profoundly affected the flow. The single cylinder produced a "textbook" vortex street (see Fig. 22) at both Mach numbers. This flow was characterized via the hot film at a Mach number of .1 using the test locations shown in Table III. Representative results are shown in Figure 23. The hot film data shows a pattern which almost perfectly mimics that of a sinusoid (see Figs. 5 - 7). The

Figure 22. Schlieren Photograph of von Karman Vortex Street, M = .6 .

TABLE III

HOT FILM MEASUREMENT TEST POINTS FOR VON KÁRMÁN VORTEX STREET

Test Point	Centerline Axial Location	Centerline Lateral Location
1	9 1/2D	-2 1/2D
2	9 1/2D	-2D
3	9 1/2D	-1 1/2D
4	9 1/2D	-1D
5	9 1/2D	-1/2D
6	9 1/2D	0D
7	9 1/2D	1/2D
8	9 1/2D	1D
9	9 1/2D	1 1/2D
10	9 1/2D	2D
11	9 1/2D	2 1/2D
12	12D	2 1/2D
13	12D	2D
14	12D	1 1/2D
15	12D	1D
16	12D	1/2D
17	12D	0D
18	12D	-1/2D
19	12D	-1D
20	12D	-1 1/2D
21	12D	-2D
22	12D	-2 1/2D

autocorrelation information shows obvious periodicity while the power spectral density plots depict one predominant frequency of approximately 860 Hz. This compares favorably with the frequency determined from Eq. 1 and Fig. 1. The full set

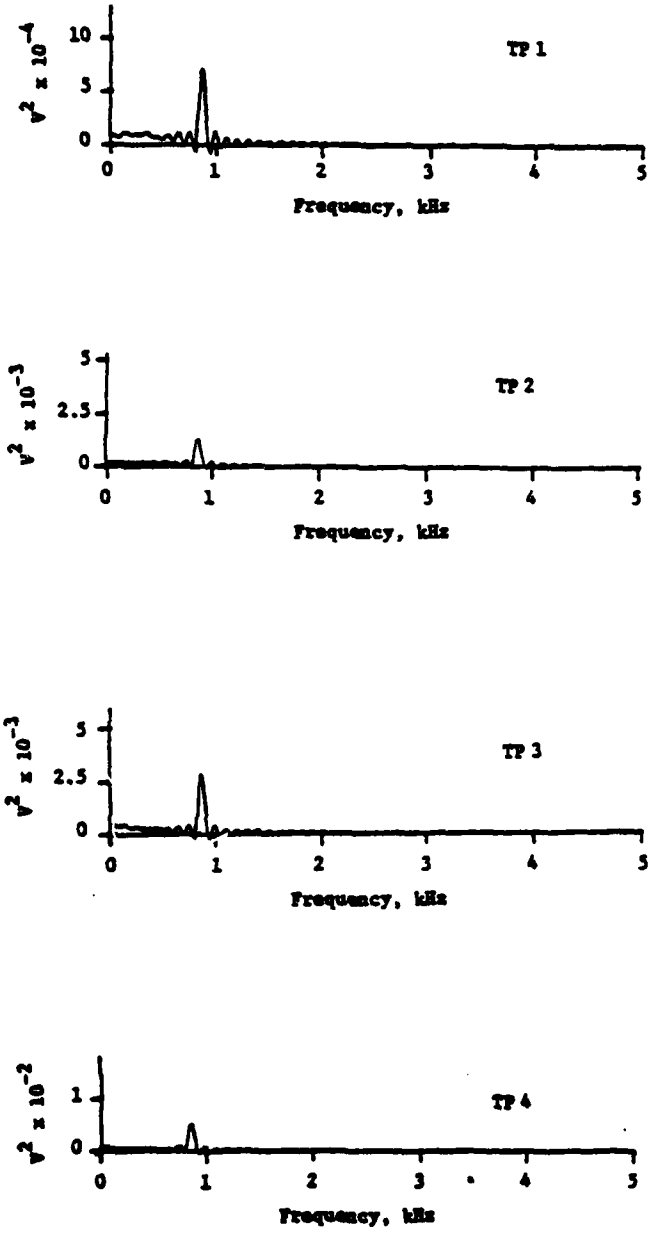

Figure 23. Power Spectral Density Plots of von Kármán Vortex Street at M = .1 (TP 1 - TP 4).

of data is presented in Appendix C. The configuration was also run with two cylinders, and except for obvious wall effects, the vortex streets appear to be unaffected by the presence of the additional cylinder. The only possible effect is in the phase of the vortex shedding. They appear to be shed in phase as can be observed in Figure 24.

An important point should be noted about these findings. Although vortex street information is ubiquitous in the literature, nowhere is it mentioned that an enclosed channel is needed to form the streets when using a free jet under the conditions of this study. The data obtained from this research appears to indicate that a duct is necessary for a classical vortex street to form in a free jet flow field. However, close examination of the flow field created using cylinder diameters of .033 cm shown by Weston (Ref 5: 42) indicates that possibly a free jet is capable of producing vortex streets behind extremely small diameter cylinders. Thus, it seems that the near proximity of the free jet flow field interacting with the stagnant surrounding air somehow overpowers the type of instability which permits the alternate shedding of vortices. This concept then supports both the results of this research and why observations have been made of classical vortex streets being formed from telephone lines and wind gusts.

A system error of 2% was attributed to hot film reproducibility/calibration curve/manometer setting error. A 2%

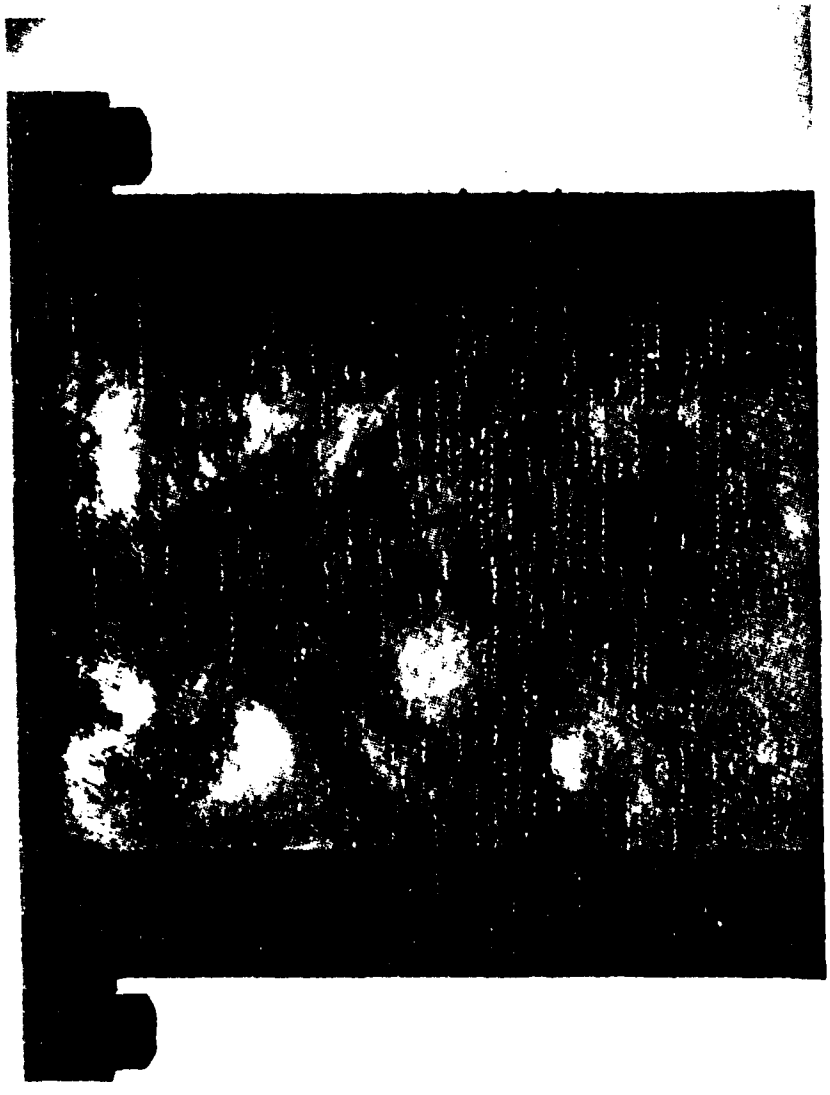

Figure 24. Schlieren Photograph of Two von Karman Vortex Streets at M = .6 .

error was also assumed for the correlator and spectrum display. This gave a minimum total anemometer data measurement system error of 4%. The actual error determined from the frequency obtained by the power spectral density plots and the frequency predicted by Eq. 1 and Fig. 1 was less than 1%.

The velocity used in Eq. 4 was determined from stagnation temperature. Since the local velocity depends on local temperature, calculations for velocity were not exact. At M = .6 conditions, a 3% error occurred which had no significant effect upon the schlieren photographs. At M = .1 conditions, less than 1/2% error in velocity produced negligible errors. Thus, for this study, use of a slightly inaccurate velocity in Eq. 4 did not lead to significant errors.

VI. Conclusions

Several conclusions can be drawn based on the von Kármán vortex streets observed in the water tunnel and various patterns produced by the free jet and its modifications. The hot film measurement data helped substantiate the results obtained by schlieren photography leading to the following conclusions:

1. The schlieren photographs and the hot film measurements verified the formation of a von Kármán vortex street in the ducted free jet flow with a three-dimensional nozzle and channel attachment. The vortex street was not present unless the channel attachment was used. Thus, the formation of a vortex street of visible size by a free jet is dependent on having a duct attached to the nozzle and continuing downstream of the .794 cm cylinder.
2. For $Re_D < 1 \times 10^4$, the water tunnel verified that von Kármán vortex streets appeared behind cylinders placed 2 to 6 diameters apart and having 0 to 2 diameters streamwise separation. The formation of these vortex streets then indicated that a diverging dead wake pattern similar to that produced by the free jet could not be generated in the water tunnel with a constant area duct by another cylinder present within 6 diameters.

3. The hot film anemometer measurement system verified the vortex shedding frequency in the third configuration to within 1% of the predicted theoretical value. The frequency and correlation data showed the strong periodicity, characteristic of the von Kármán vortex street, through 12 diameters downstream of the cylinder.
4. The free jet produced diverging dead wake patterns behind cylinders with separation distances of 2 to 6 diameters. It can be inferred from this and conclusion 1 above that the formation of a von Kármán vortex street by a free jet is not dependent on adjacent cylinder location for $Re_D \leq 1.1 \times 10^5$.
5. A turbulent grid consisting of more than one von Kármán vortex street is possible using the free jet if the channel attachment is used. Cylinder diameters less than .794 cm would be necessary to obtain non-overlapping vortex streets within the 5 cm square channel.

VII. Recommendations

The efforts of this study as well as the results can be used as a starting point for further research or as a continuation of this study. Several recommendations can be made as suggestions of possible topics or directions of research:

1. Build a permanent water tunnel with low turbulence characteristics. The recently procured water pump can be used as a basis for the new tunnel. A dye injection capability would be imperative for flow visualization studies. Low turbulence measurements would be needed for validation of the water tunnel flow field quality.
2. Create a turbulent grid flow field using the modified free jet for laser beam degradation studies. A laser beam intensity study based on turbulent grid densities could then be investigated.
3. Investigate the effects of a duct and near boundaries on the formation of the von Kármán vortex street. This study could include the formation of small vortex streets using the original free jet configuration.
4. Investigate the turbulence level of the 5 cm by 5 cm square nozzle using hot wire/film measurements.
5. Analytically derive the vortex street pattern. Numerical schemes and computational aerodynamics techniques could be used to model the flow field.

Appendix A

Modifications Made to the Cylinder and Free Jet Nozzle

The modifications made to the test cylinder and nozzle that follow were tested in the order presented. Most modifications had little or no effect on the flow field pattern.

1. Heated cylinder -- The single cylinder was heated using a portable propane torch for several minutes just prior to flow initiation; no effect.
2. 1.27 cm spacers with one cylinder -- Same type of spacers as those in Figure 10; no effect.
3. 1.59 cm spacers with one cylinder -- See Figure 10; no effect.
4. 1.905 cm spacers with one cylinder -- See Figure 10; narrow wake pattern.
5. 1.905 cm spacers with two cylinders having 8 diameters separation -- Narrow wake pattern.
6. 1.905 cm spacers with two cylinders having 6 diameters separation -- Narrow wake pattern.
7. 1.905 cm spacers with two cylinders having 4 diameters separation -- Narrow wake pattern.
8. Chopped cylinder -- The back portion of the cylinder was cut away as shown in Figure 25; no effect.
9. Flat plate -- The front and back portions of the

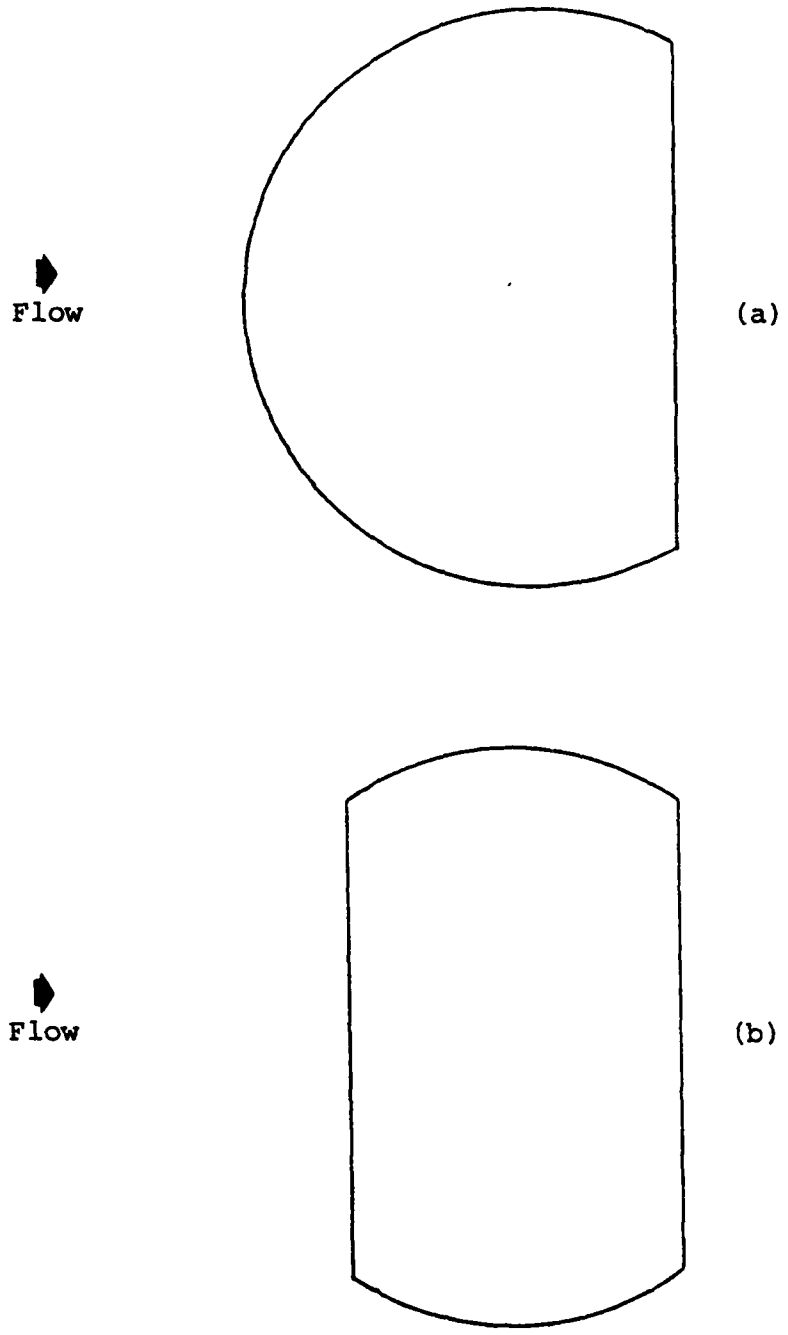

Figure 25. Cylinder Modifications. (a) Chopped Cylinder, (b) Flat Plate.

cylinder were cut away as shown in Figure 25; wide wake pattern.

10. Two chopped cylinders having 8 diameters separation -- no effect.
11. Two flat plates having 8 diameters separation -- wide wake pattern.
12. Two chopped cylinders having 6 diameters separation -- no effect.
13. 2.54 cm spacers with one cylinder -- no effect.
14. 3.175 cm spacers with one cylinder -- no effect.
15. 2.54 cm spacers with one chopped cylinder -- no effect.
16. 3.175 cm spacers with one chopped cylinder -- no effect.
17. 2.54 cm spacers with one flat plate -- no effect.
18. 1.905 cm spacers with one cylinder having sandpaper attached to insure a tripped boundary layer -- no effect.
19. Helium injection cylinder with one exit port (for M = .1) -- no effect.
20. Helium injection cylinder with 5 exit ports (for M = .1) -- See Fig. 11; no effect.
21. Helium injection cylinder with exit slot (.079 cm x 2.54 cm) -- no effect.
22. One cylinder with 5 cm by 5 cm jet nozzle -- no effect.

23. 1.27 cm spacers with one cylinder attached to 5 cm square nozzle -- no effect.
24. 1.59 cm spacers with one cylinder attached to 5 cm square nozzle -- no effect.
25. 1.905 cm spacers with one cylinder attached to 5 cm square nozzle -- narrow wake pattern.
26. 1.905 cm spacers with one cylinder reverse mounted to 5 cm square nozzle -- narrowest wake pattern.
27. 12.7 cm channel attached to one cylinder plate -- vortex street.
28. 12.7 cm channel attached to two cylinder plate with 3 diameters separation -- vortex streets.

Appendix B

Hot Film Measurements for the Single Cylinder Extended 1.905 cm from the Jet Exit Plane

The data is labeled by test point location as shown in Table II. The autocorrelation information is presented first followed by the power spectral density plots for each test point.

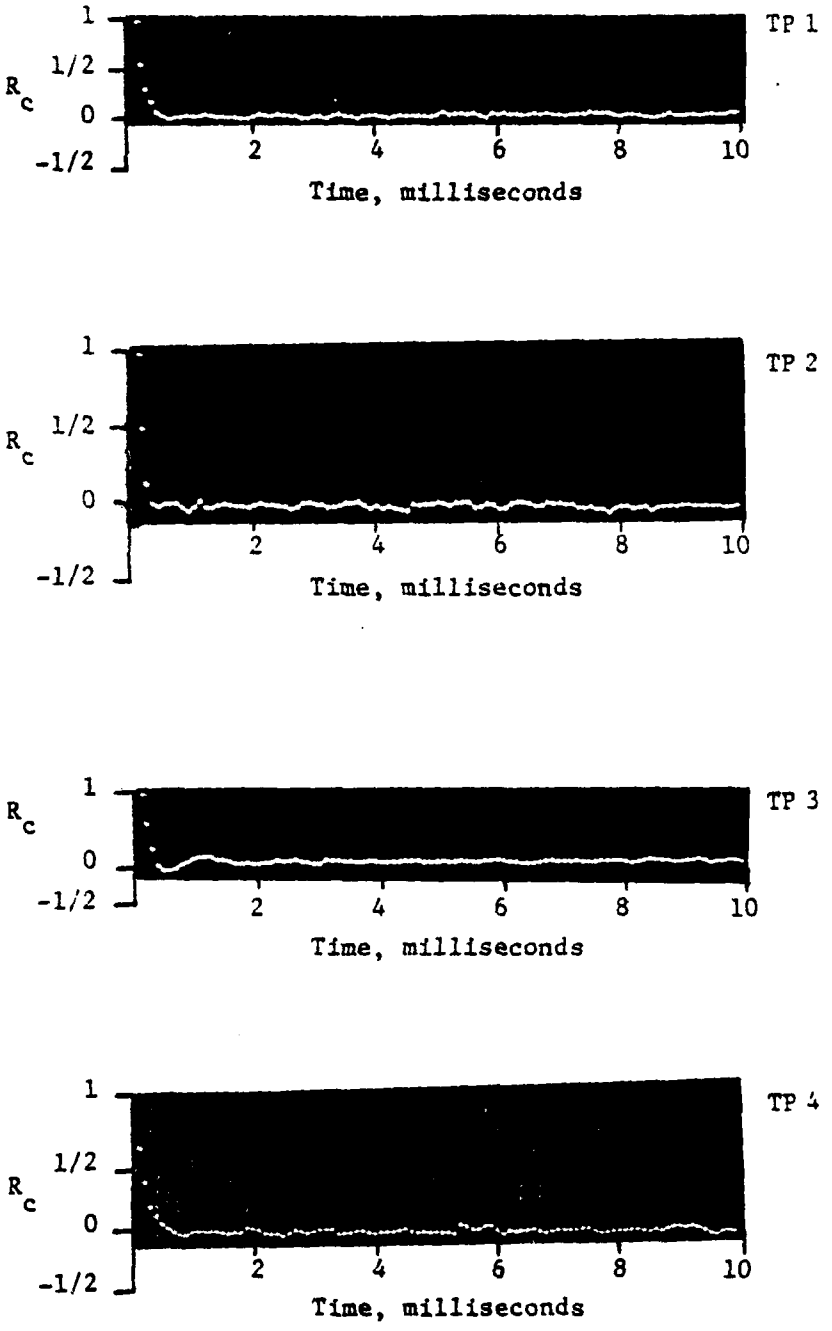

Figure 26. Autocorrelation Functions for the Single Cylinder in the Free Jet Flow Field at M = .1 (TP 1 - TP 4).

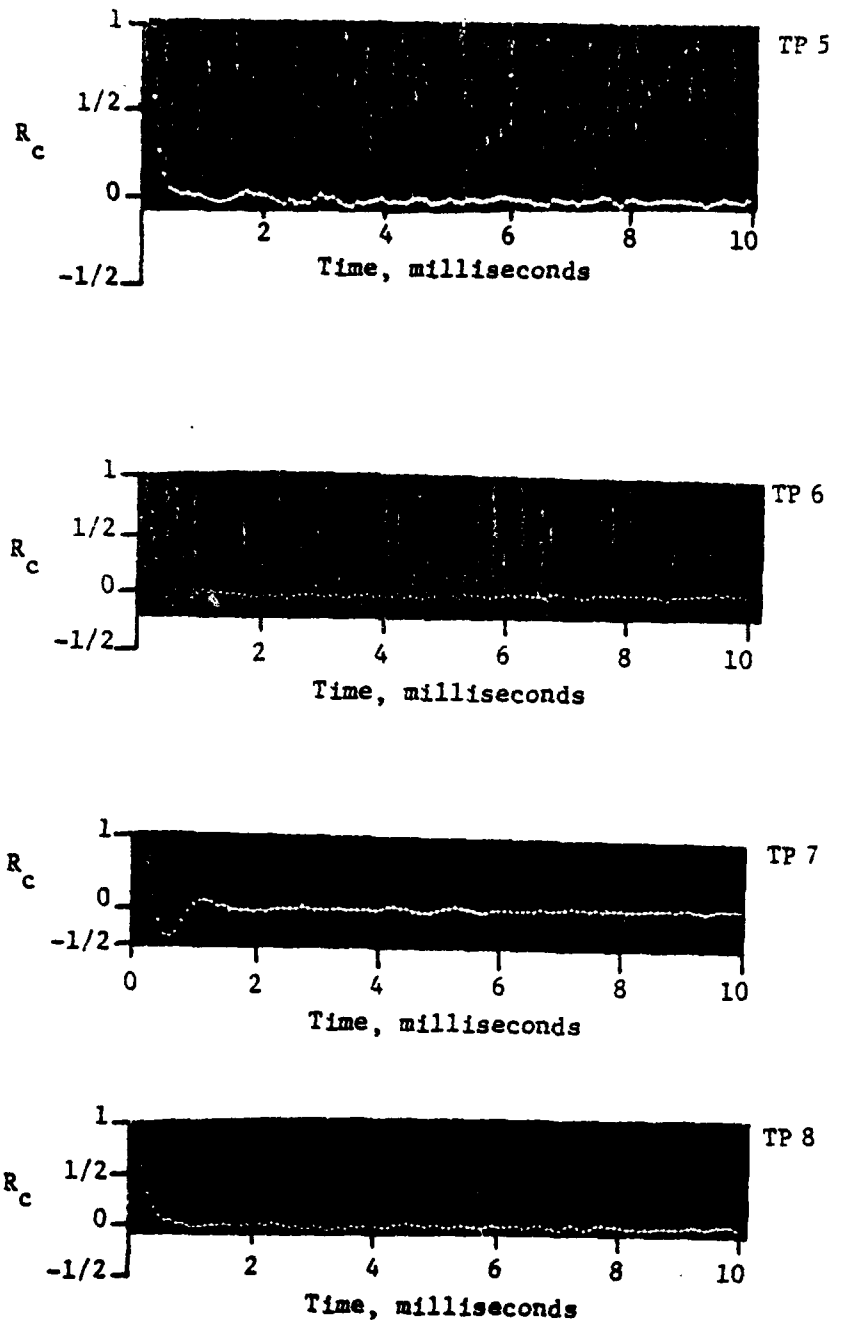

Figure 27. Autocorrelation Functions for the Single Cylinder in the Free Jet Flow Field at M = .1 (TP 5 - TP 8).

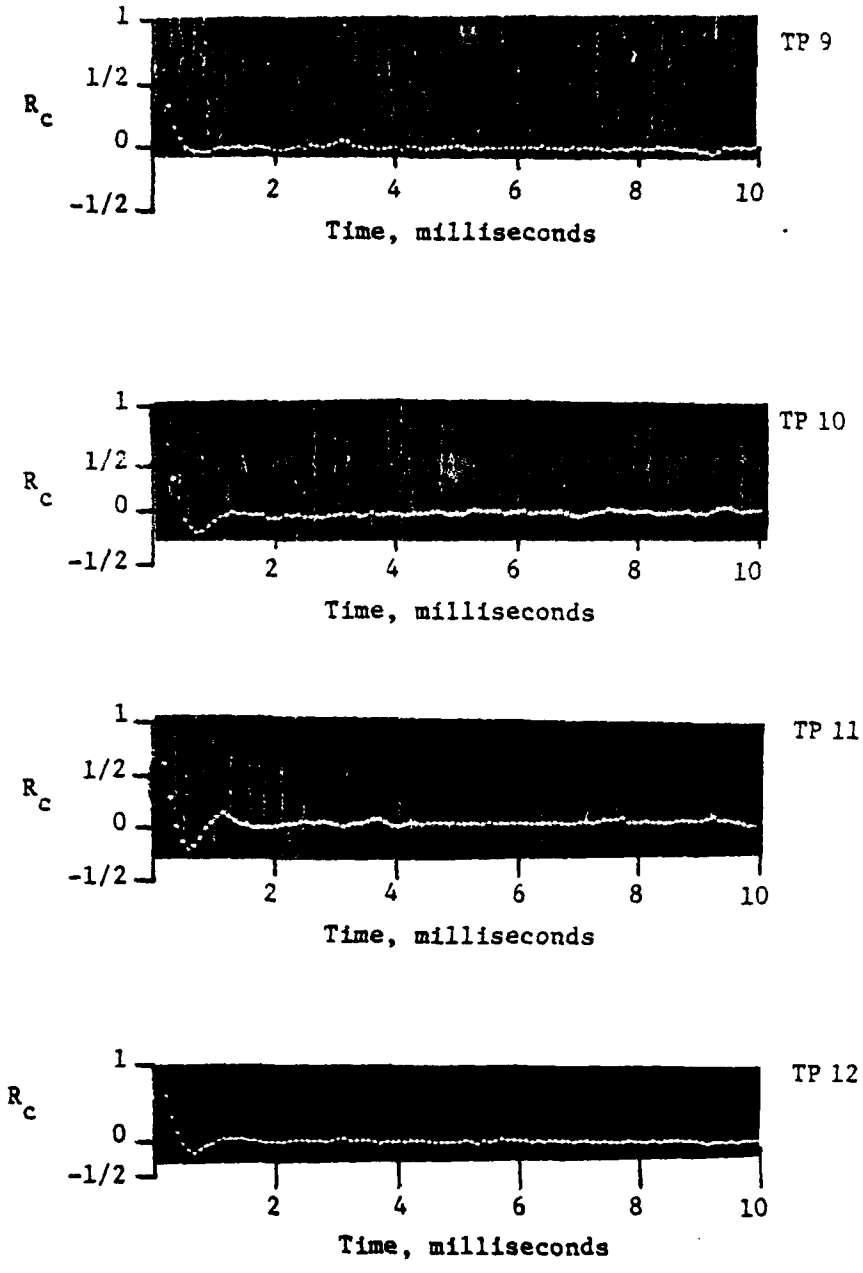

Figure 28. Autocorrelation Functions for the Single Cylinder in the Free Jet Flow Field at M = .1 (TP 9 - TP 12).

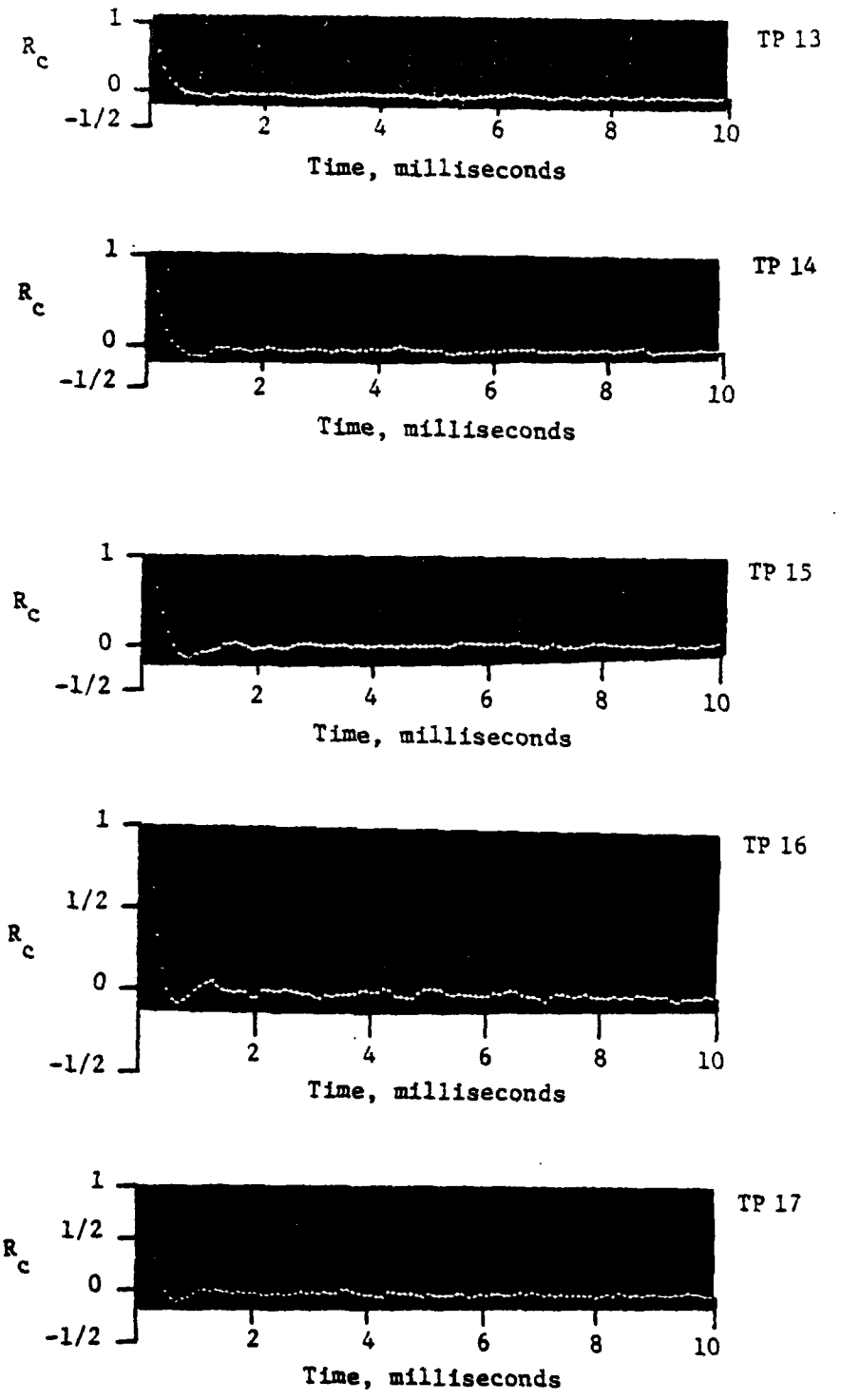

Figure 29. Autocorrelation Functions for the Single Cylinder in the Free Jet Flow Field at M = .1 (TP 13 - TP 17).

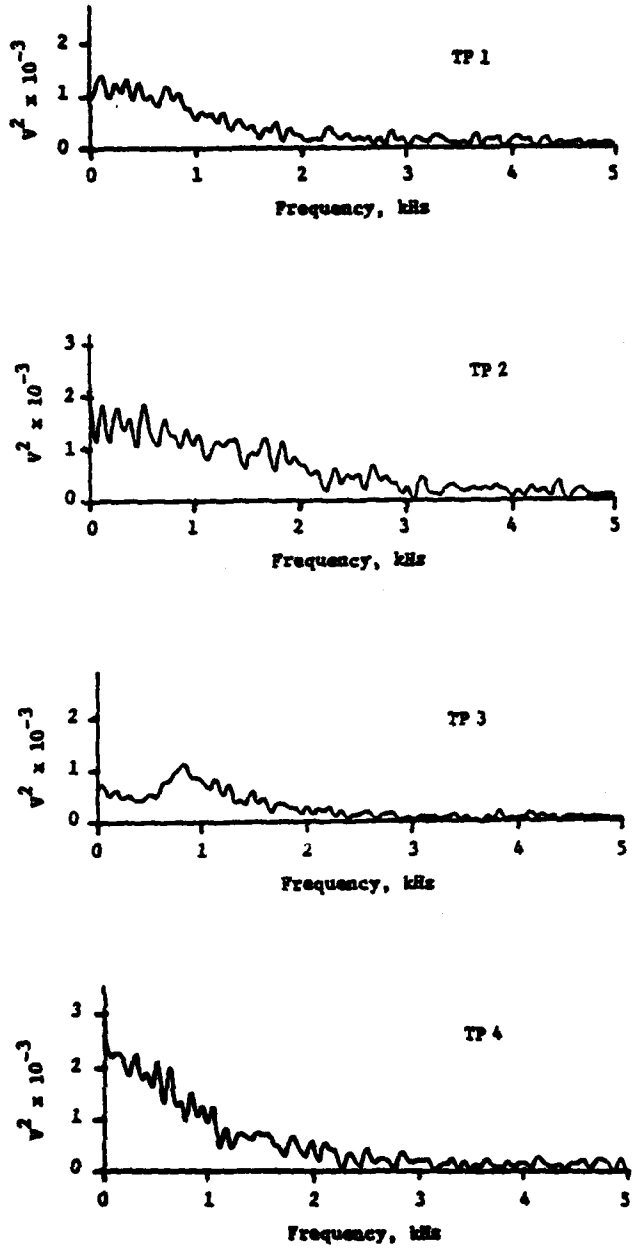

Figure 30. Power Spectral Density Plots for the Single Cylinder in the Free Jet Flow Field at M = .1 (TP 1 - TP 4).

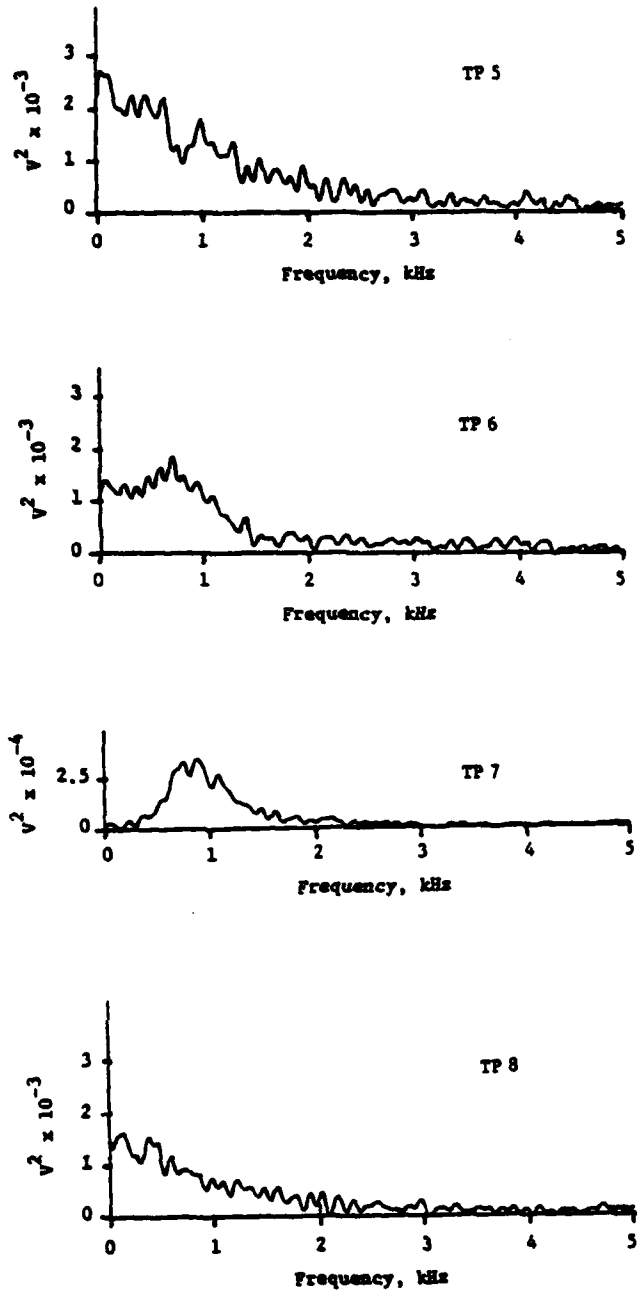

Figure 31. Power Spectral Density Plots for the Single Cylinder in the Free Jet Flow Field at M = .1 (TP 5 - TP 8).

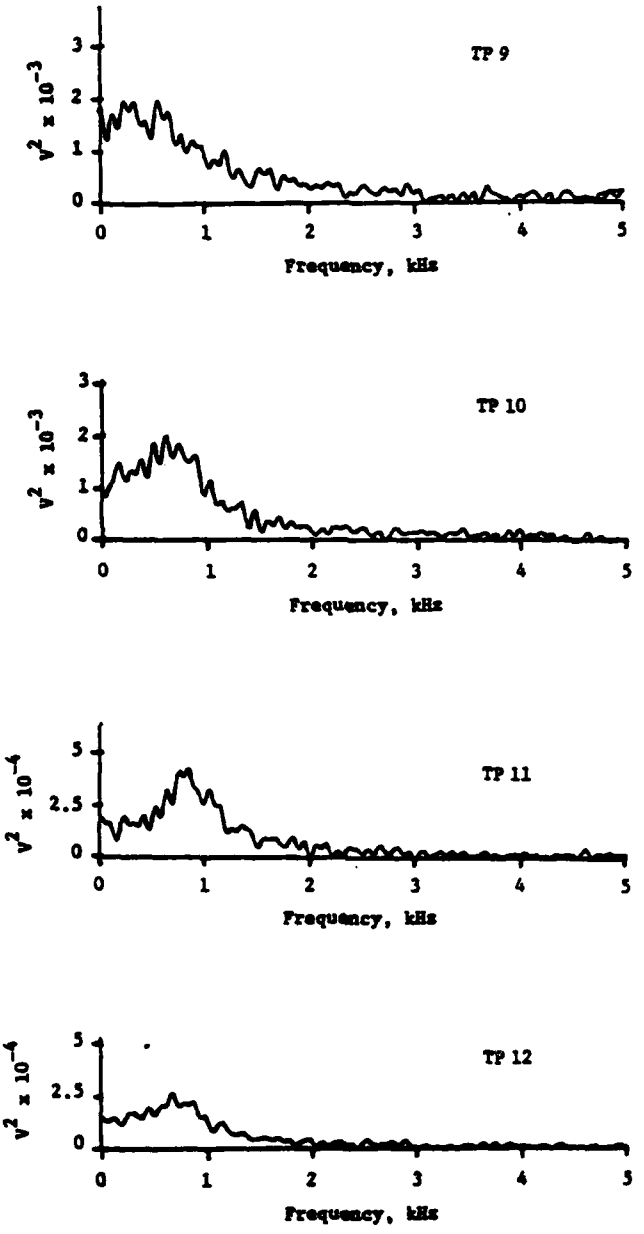

Figure 32. Power Spectral Density Plots for the Single Cylinder in the Free Jet Flow Field at M = .1 (TP 9 - TP 12).

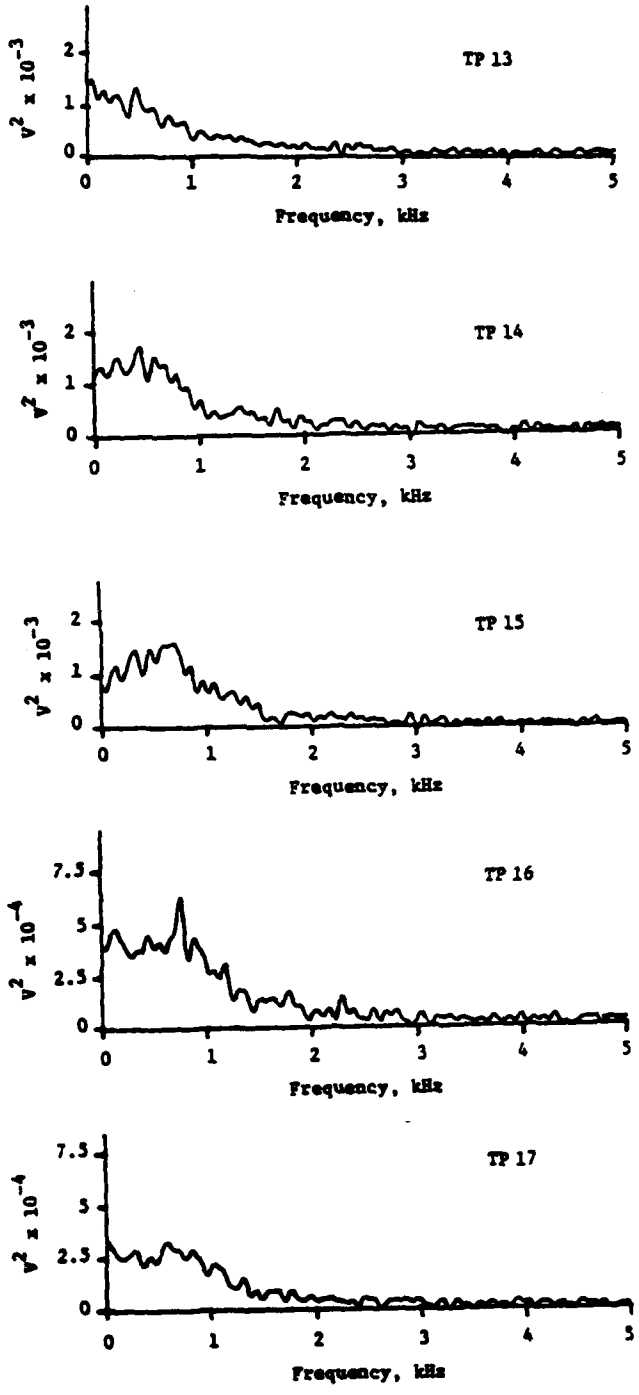

Figure 33. Power Spectral Density Plots for the Single Cylinder in the Free Jet Flow Field at M = .1 (TP 13 - TP 17).

Appendix C

Hot Film Measurements of the von Karman Vortex Street

The data is labeled by test point location as shown in Table III. The autocorrelation information is presented first followed by the power spectral density plots for each test point.

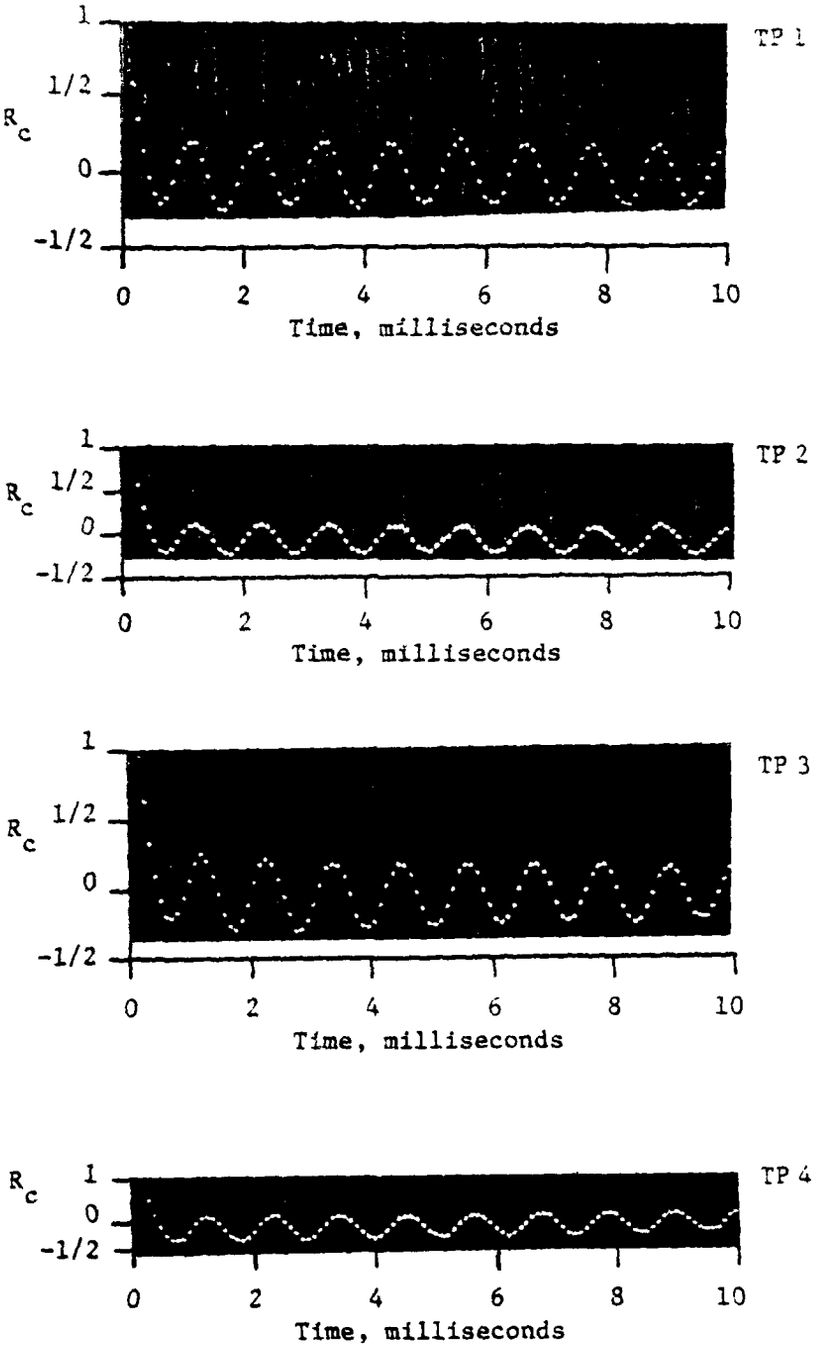

Figure 34. Autocorrelation Functions for the von Karman Vortex Street at M = .1 (TP 1 - TP 4).

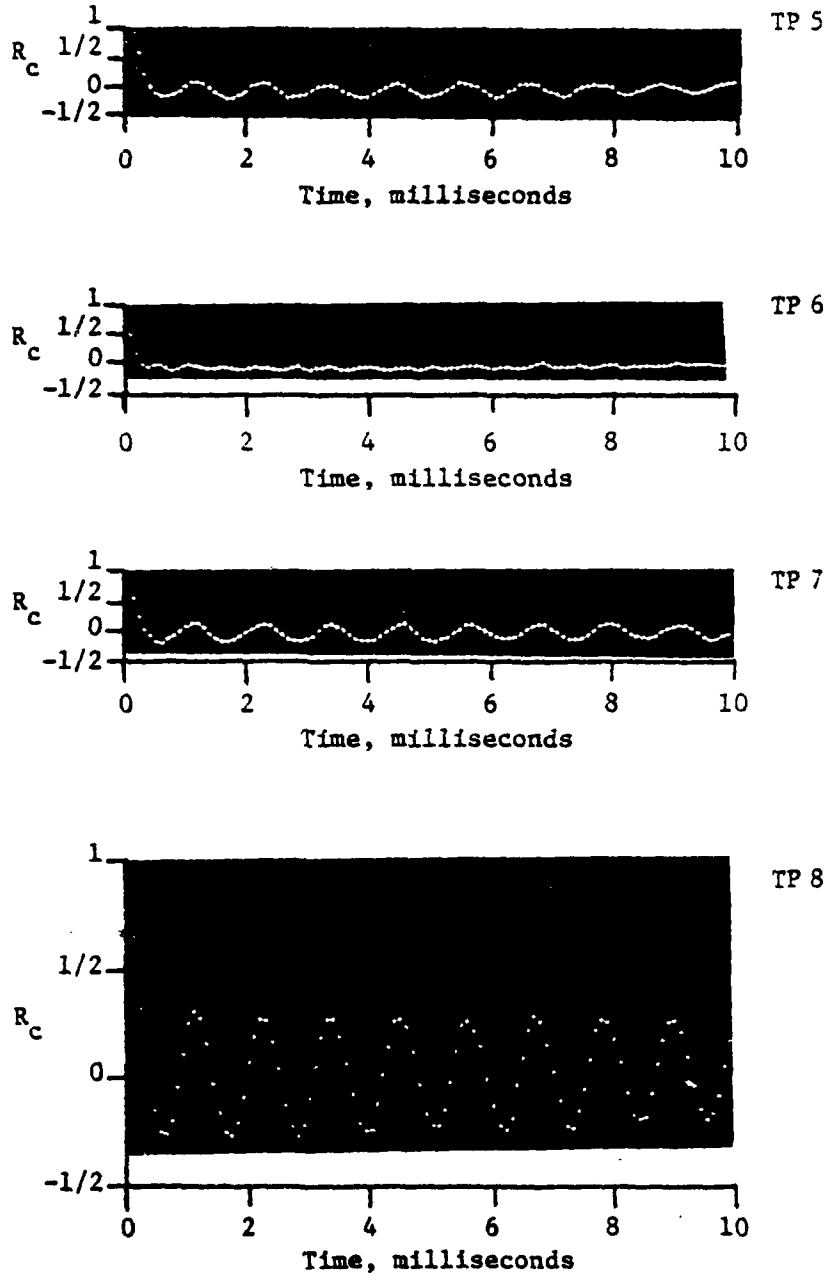

Figure 35. Autocorrelation Functions for the von Kármán Vortex Street at M = .1 (TP 5 - TP 8).

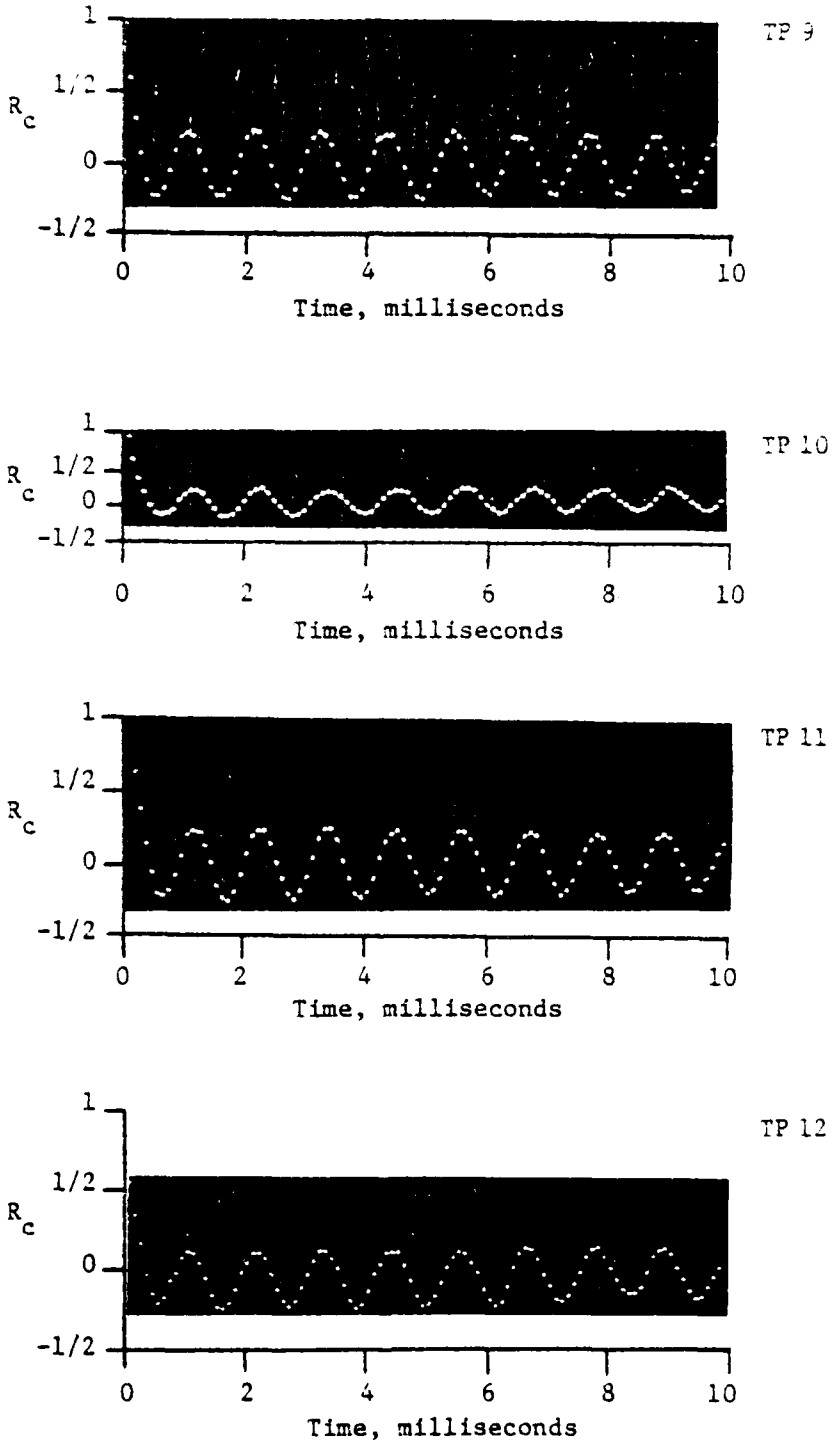

Figure 36. Autocorrelation Functions for the von Karman Vortex Street at M = .1 (TP 9 - TP 12).

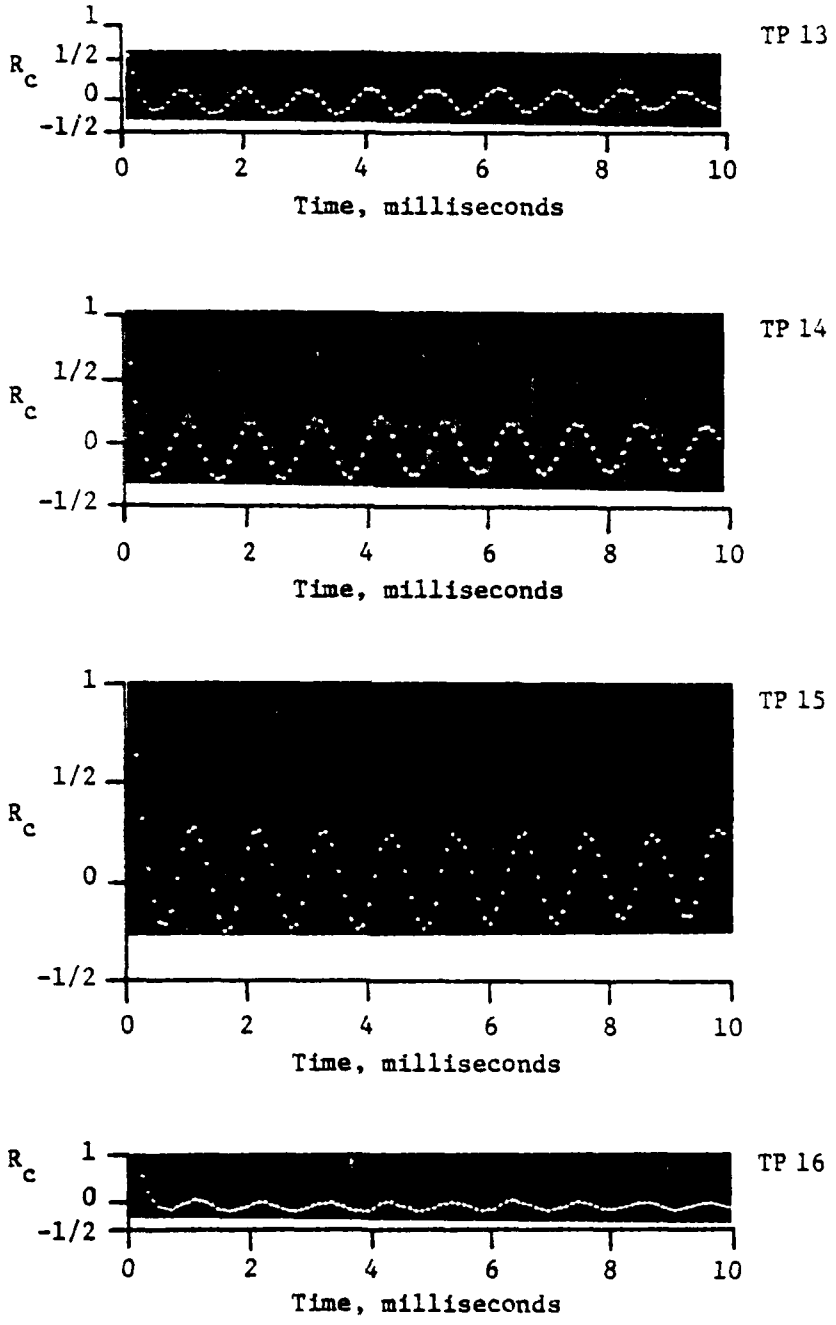

Figure 37. Autocorrelation Functions for the von Karman Vortex Street at M = .1 (TP 13 - TP 16).

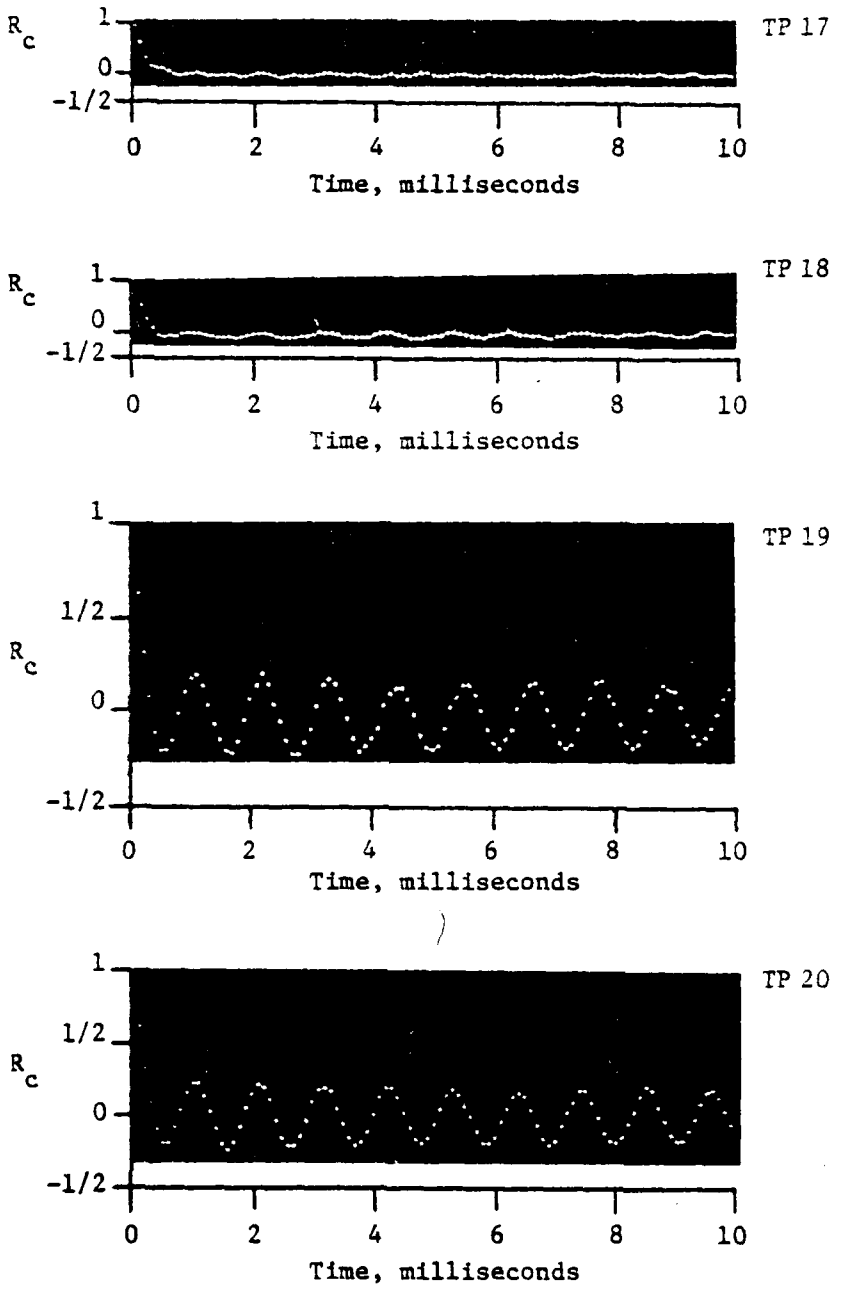

Figure 38. Autocorrelation Functions for the von Karman Vortex Street at M = .1 (TP 17 - TP 20).

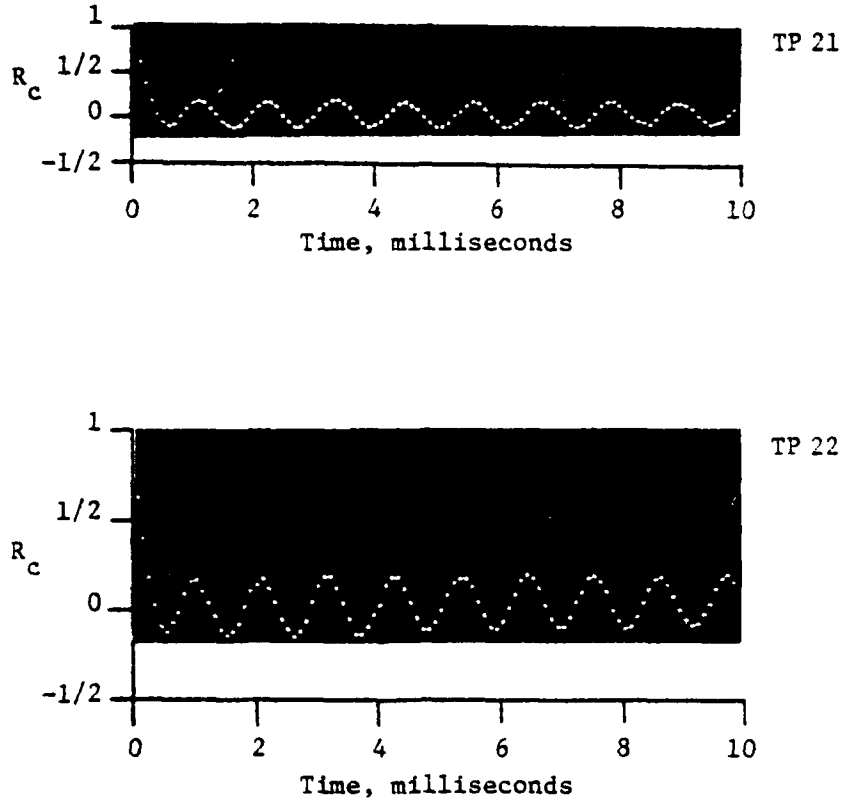

Figure 39. Autocorrelation Functions for the von Karman Vortex Street at M = .1 (TP 21 - TP 22).

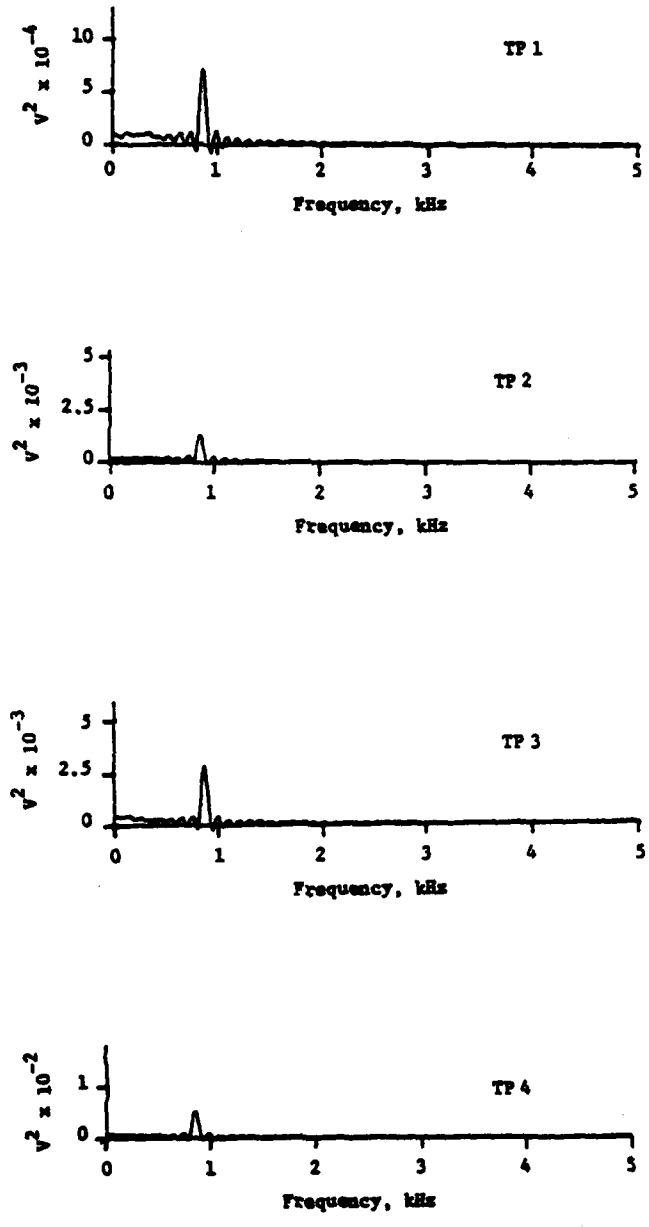

Figure 40. Power Spectral Density Plots for the von Kármán Vortex Street at M = .1 (TP 1 - TP 4).

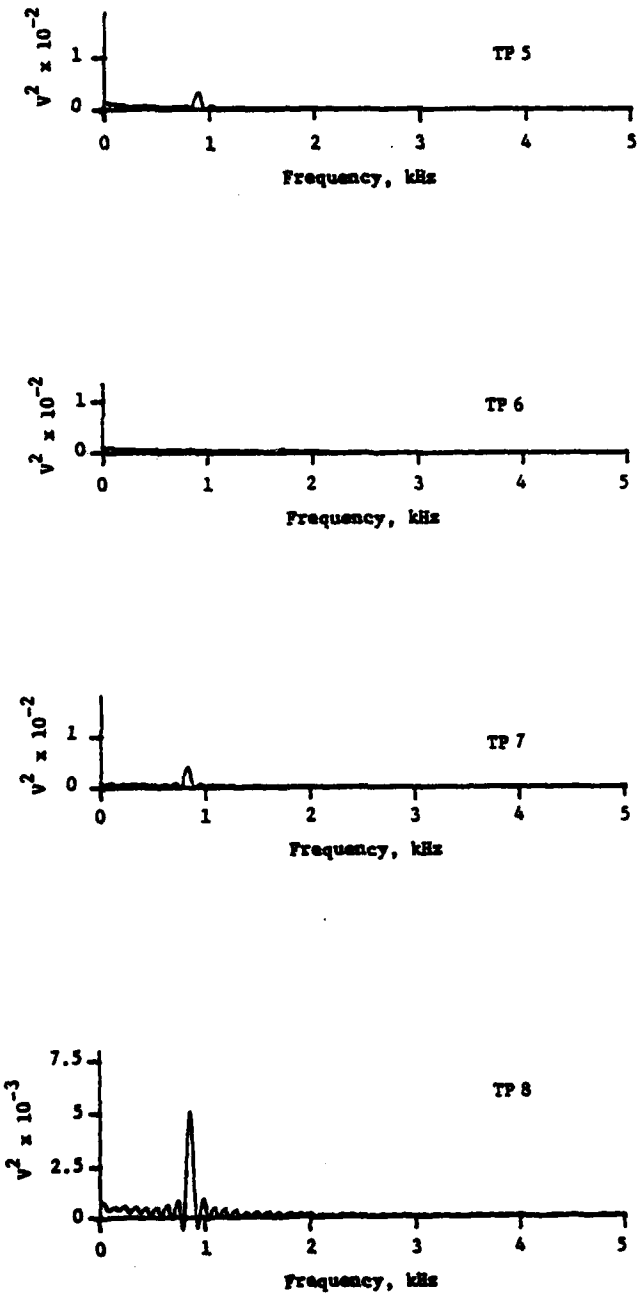

Figure 41. Power Spectral Density Plots for the von Kármán Vortex Street at M = .1 (TP 5 - TP 8).

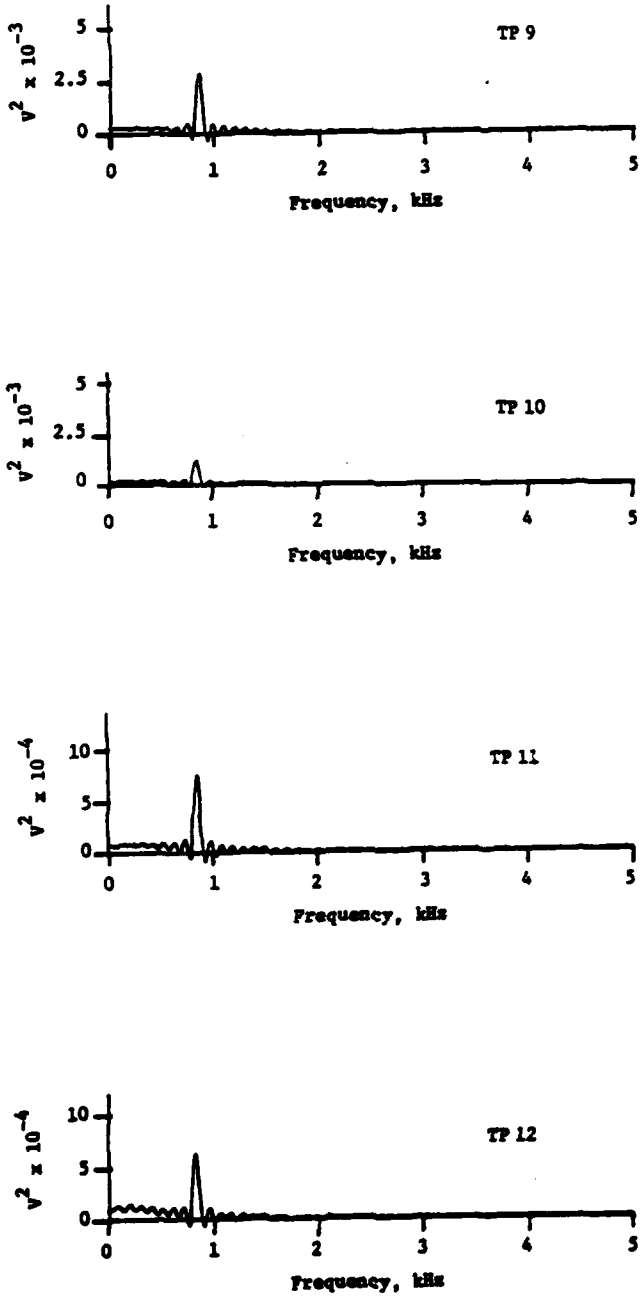

Figure 42. Power Spectral Density Plots for the von Kármán Vortex Street at M = .1 (TP 9 - TP 12).

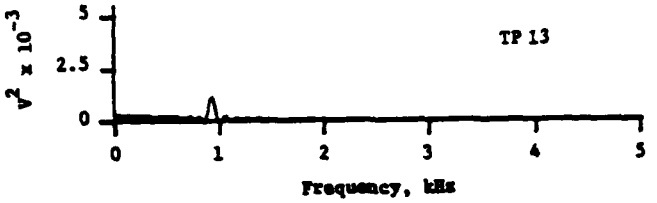

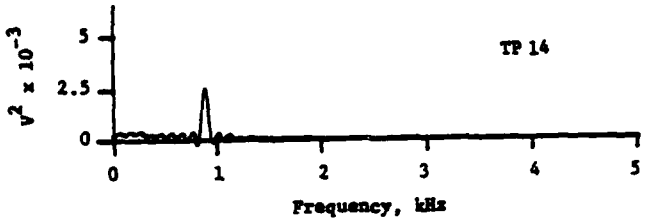

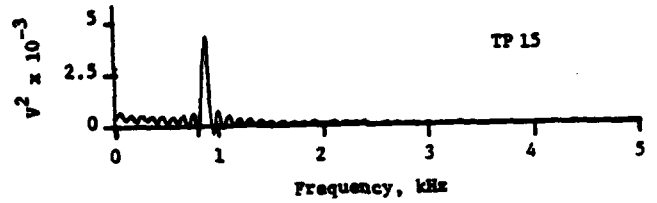

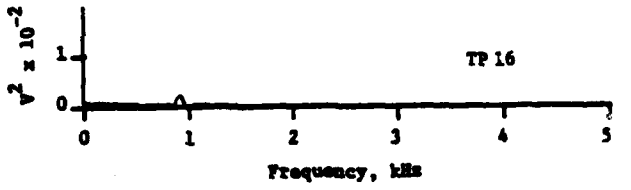

Figure 43. Power Spectral Density Plots for the von Kármán Vortex Street at M = .1 (TP 13 - TP 16).

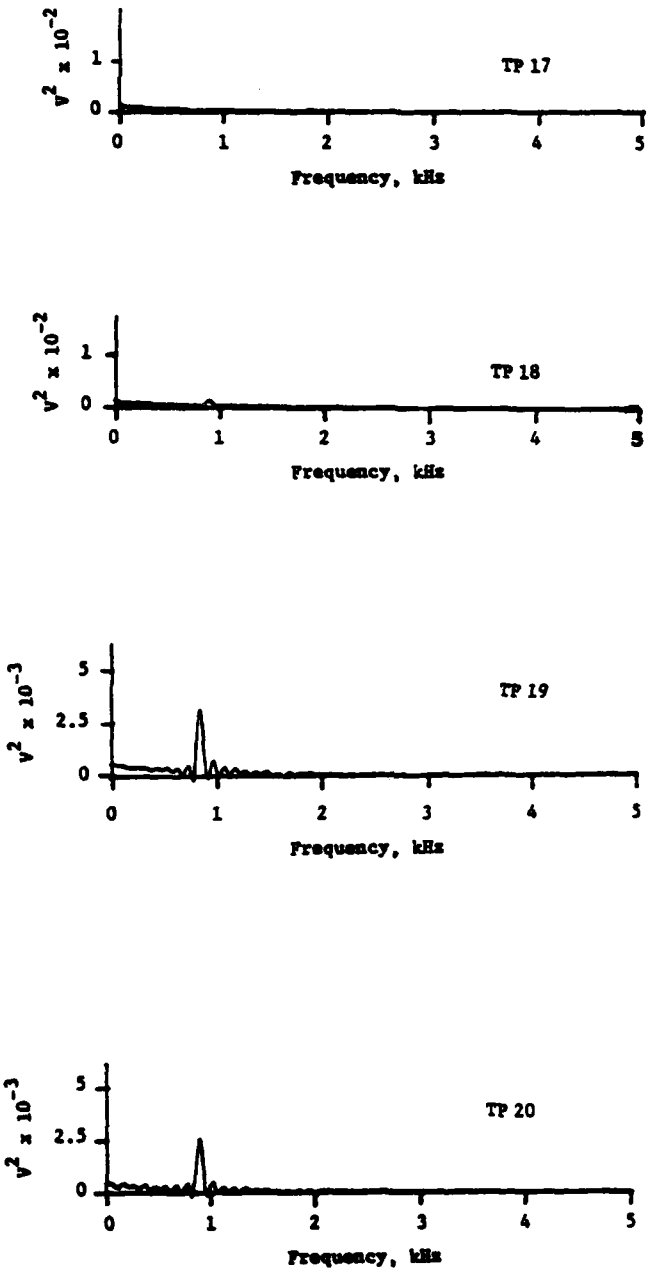

Figure 44. Power Spectral Density Plots for the von Kármán Vortex Street at M = .1 (TP 17 - TP 20).

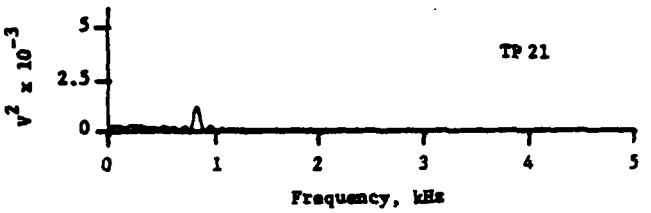

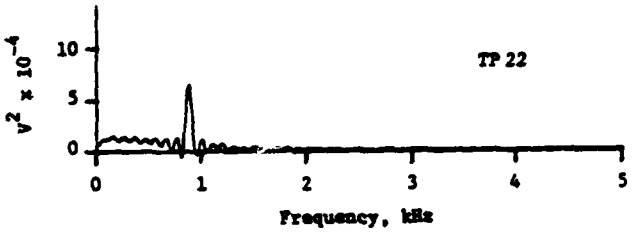

Figure 45. Power Spectral Density Plots for the von Kármán Vortex Street at M = .1 (TP 21 - TP 22).

Bibliography

1. Wille, R. "Karman Vortex Streets," Advances in Applied Mechanics, Vol. VI, edited by G. Kuerti. New York: Academic Press, 1960.

2. Morkovin, M. V. "Flow About a Circular Cylinder -- A Kaleidoscope of Challenging Fluid Phenomena". Symposium on Fully Separated Flows. ASME: 102-118. New York, New York, 1964.

3. Abernathy, F. and Kronauer, R. "The Formation of Vortex Streets," Journal of Fluid Mechanics, 13: 1-20 (May 1962).

4. Roshko, A. "On the Development of Turbulent Wakes from Vortex Streets". Fortieth Annual Report of the NACA: 801-825, NACA TR 1191. U. S. Government Printing Office, 1956.

5. Weston, C. P. Influence of Periodic Compressible Vortices on Laser Beam Intensity. M.S. Thesis. Wright-Patterson Air Force Base, Ohio: Air Force Institute of Technology, December 1982.

6. Jumper, E. J. Personal communication. School of Engineering, Air Force Institute of Technology, Wright-Patterson Air Force Base, Ohio. December, 1982.

7. Shepard, W. K. Turbulence Measurements in a Plane Free Jet at High Subsonic Velocities. M.S. Thesis. Wright-Patterson Air Force Base, Ohio: Air Force Institute of Technology, December 1974.

8. Kirchner, M. J. Computer Assisted Velocity and Turbulence Measurements in a Plane Free Jet at High Subsonic Velocities. M.S. Thesis. Wright-Patterson Air Force Base, Ohio: Air Force Institute of Technology, December 1981.

9. McErlean, D. P. et al. Water Table Simulation of Subsonic Channel Flow, AFAPL-TR-72-37. Wright-Patterson Air Force Base, Ohio: Air Force Aero Propulsion Laboratory, June 1972.

10. Schlicting, H. Boundary Layer Theory. New York: McGraw-Hill Co., 1979.

11. Van Dyke, M. An Album of Fluid Motion. Stanford: Parabolic Press, 1982.

12. Morris, S. L. A Diagnostic Study of Flow in the Wake of a Circular Disk Using a Photon Correlation Laser Velocimeter. M.S. Thesis. Wright-Patterson Air Force Base, Ohio: Air Force Institute of Technology, March 1980.

13. Bendat, J. S. and Piersol, A. G. Measurement and Analysis of Random Data. New York: Wiley and Sons, 1966.

14. Bruce, P. W. Flow Visualization in Axial-Flow Compressor and Turbine Cascades Utilizing the Water Table. M.S. Thesis. Wright-Patterson Air Force Base, Ohio: Air Force Institute of Technology, December 1973.

15. Baird, J. Design of Choking Cascade Turns. M.S. Thesis. Wright-Patterson Air Force Base, Ohio: Air Force Institute of Technology, December 1982.

16. Thermo-Systems, Inc. Instruction Manual for Model 1050 Anemometer. St. Paul, Minnisota: Thermo-Systems, Inc.

17. Cox, W. R. Personal communication. School of Engineering, Air Force Institute of Technology, Wright-Patterson Air Force Base, Ohio. June, 1983.

VITA

Gary F. Clark was born 11 May 1952 in Sharon, Connecticut. He graduated from Dover High School, Dover Plains, New York in 1970 and completed one year of school at Florida Institute of Technology, Melbourne, Florida before entering the United States Military Academy at West Point. He received his Bachelor of Science Degree in Engineering and a commission in the U.S. Army upon graduation from the Academy in 1975. He completed Ranger School and served 5 1/2 years in the Army as a Field Artillery Officer at Fort Carson, Colorado; Chun Chon, Korea; and Fort Sill, Oklahoma before transferring into the Air Force in 1980. After an assignment as a Project Test Engineer in the Flight Dynamics Laboratory at Wright-Patterson Air Force Base, he entered the Graduate Aeronautical Engineering Program at the Air Force Institute of Technology in June 1982.

Permanent Address: Route 22
Dover Plains, New York 12522

AD-A136 930 EFFECTS OF MULTIPLE CYLINDERS ON THE FORMATION OF VON KARMAN VORTEX STREETS(U) AIR FORCE INST OF TECH WRIGHT-PATTERSON AFB OH SCHOOL OF ENGI.. G F CLARK

UNCLASSIFIED DEC 83 AFIT/GAE/ENY/83D-5 F/G 20/4 NL

2/2

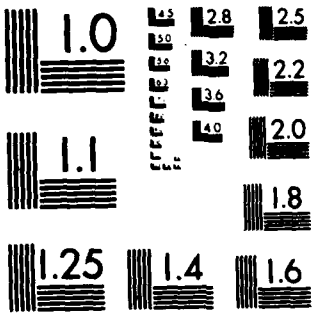
1.0
1.1
1.25
1.4
1.6
1.8
2.0
2.2
2.5
2.8
3.2
3.6
4.0
4.5
5.0
5.6
6.3
7.1
8.0
9.0
10.0
11.2
12.5
14.0
16.0
18.0
20.0
22.4
25.0
28.0
32.0
36.0
40.0
45.0
50.0
56.0
63.0
71.0
80.0
90.0
100.0
112.0
125.0
140.0
160.0
180.0
200.0
224.0
250.0
280.0
320.0
360.0
400.0
450.0
500.0
560.0
630.0
710.0
800.0
900.0
1000.0
1120.0
1250.0
1400.0
1600.0
1800.0
2000.0
2240.0
2500.0
2800.0
3200.0
3600.0
4000.0
4500.0
5000.0
5600.0
6300.0
7100.0
8000.0
9000.0
10000.0
11200.0
12500.0
14000.0
16000.0
18000.0
20000.0
22400.0
25000.0
28000.0
32000.0
36000.0
40000.0
45000.0
50000.0
56000.0
63000.0
71000.0
80000.0
90000.0
100000.0
112000.0
125000.0
140000.0
160000.0
180000.0
200000.0
224000.0
250000.0
280000.0
320000.0
360000.0
400000.0
450000.0
500000.0
560000.0
630000.0
710000.0
800000.0
900000.0
1000000.0
1120000.0
1250000.0
1400000.0
1600000.0
1800000.0
2000000.0
2240000.0
2500000.0
2800000.0
3200000.0
3600000.0
4000000.0
4500000.0
5000000.0
5600000.0
6300000.0
7100000.0
8000000.0
9000000.0
10000000.0
11200000.0
12500000.0
14000000.0
16000000.0
18000000.0
20000000.0
22400000.0
25000000.0
28000000.0
32000000.0
36000000.0
40000000.0
45000000.0
50000000.0
56000000.0
63000000.0
71000000.0
80000000.0
90000000.0
100000000.0
112000000.0
125000000.0
140000000.0
160000000.0
180000000.0
200000000.0
224000000.0
250000000.0
280000000.0
320000000.0
360000000.0
400000000.0
450000000.0
500000000.0
560000000.0
630000000.0
710000000.0
800000000.0
900000000.0
1000000000.0
1120000000.0
1250000000.0
1400000000.0
1600000000.0
1800000000.0
2000000000.0
2240000000.0
2500000000.0
2800000000.0
3200000000.0
3600000000.0
4000000000.0
4500000000.0
5000000000.0
5600000000.0
6300000000.0
7100000000.0
8000000000.0
9000000000.0
10000000000.0
11200000000.0
12500000000.0
14000000000.0
16000000000.0
18000000000.0
20000000000.0
22400000000.0
25000000000.0
28000000000.0
32000000000.0
36000000000.0
40000000000.0
45000000000.0
50000000000.0
56000000000.0
63000000000.0
71000000000.0
80000000000.0
90000000000.0
100000000000.0
112000000000.0
125000000000.0
140000000000.0
160000000000.0
180000000000.0
200000000000.0
224000000000.0
250000000000.0
280000000000.0
320000000000.0
360000000000.0
400000000000.0
450000000000.0
500000000000.0
560000000000.0
630000000000.0
710000000000.0
800000000000.0
900000000000.0
1000000000000.0
1120000000000.0
1250000000000.0
1400000000000.0
1600000000000.0
1800000000000.0
2000000000000.0
2240000000000.0
2500000000000.0
2800000000000.0
3200000000000.0
3600000000000.0
4000000000000.0
4500000000000.0
5000000000000.0
5600000000000.0
6300000000000.0
7100000000000.0
8000000000000.0
9000000000000.0
10000000000000.0
11200000000000.0
12500000000000.0
14000000000000.0
16000000000000.0
18000000000000.0
20000000000000.0
22400000000000.0
25000000000000.0
28000000000000.0
32000000000000.0
36000000000000.0
40000000000000.0
45000000000000.0
50000000000000.0
56000000000000.0
63000000000000.0
71000000000000.0
80000000000000.0
90000000000000.0
100000000000000.0
112000000000000.0
125000000000000.0
140000000000000.0
160000000000000.0
180000000000000.0
200000000000000.0
224000000000000.0
250000000000000.0
280000000000000.0
320000000000000.0
360000000000000.0
400000000000000.0
450000000000000.0
500000000000000.0
560000000000000.0
630000000000000.0
710000000000000.0
800000000000000.0
900000000000000.0
1000000000000000.0
1120000000000000.0
1250000000000000.0
1400000000000000.0
1600000000000000.0
1800000000000000.0
2000000000000000.0
2240000000000000.0
2500000000000000.0
2800000000000000.0
3200000000000000.0
3600000000000000.0
4000000000000000.0
4500000000000000.0
5000000000000000.0
5600000000000000.0
6300000000000000.0
7100000000000000.0
8000000000000000.0
9000000000000000.0
10000000000000000.0
11200000000000000.0
12500000000000000.0
14000000000000000.0
16000000000000000.0
18000000000000000.0
20000000000000000.0
22400000000000000.0
25000000000000000.0
28000000000000000.0
32000000000000000.0
36000000000000000.0
40000000000000000.0
45000000000000000.0
50000000000000000.0
56000000000000000.0
63000000000000000.0
71000000000000000.0
80000000000000000.0
90000000000000000.0
100000000000000000.0
112000000000000000.0
125000000000000000.0
140000000000000000.0
160000000000000000.0
180000000000000000.0
200000000000000000.0
224000000000000000.0
250000000000000000.0
280000000000000000.0
320000000000000000.0
360000000000000000.0
400000000000000000.0
450000000000000000.0
500000000000000000.0
560000000000000000.0
630000000000000000.0
710000000000000000.0
800000000000000000.0
900000000000000000.0
1000000000000000000.0
1120000000000000000.0
1250000000000000000.0
1400000000000000000.0
1600000000000000000.0
1800000000000000000.0
2000000000000000000.0
2240000000000000000.0
2500000000000000000.0
2800000000000000000.0
3200000000000000000.0
3600000000000000000.0
4000000000000000000.0
4500000000000000000.0
5000000000000000000.0
5600000000000000000.0
6300000000000000000.0
7100000000000000000.0
8000000000000000000.0
9000000000000000000.0
10000000000000000000.0
11200000000000000000.0
12500000000000000000.0
14000000000000000000.0
16000000000000000000.0
18000000000000000000.0
20000000000000000000.0
22400000000000000000.0
25000000000000000000.0
28000000000000000000.0
32000000000000000000.0
36000000000000000000.0
40000000000000000000.0
45000000000000000000.0
50000000000000000000.0
56000000000000000000.0
63000000000000000000.0
71000000000000000000.0
80000000000000000000.0
90000000000000000000.0
100000000000000000000.0
112000000000000000000.0
125000000000000000000.0
140000000000000000000.0
160000000000000000000.0
180000000000000000000.0
200000000000000000000.0
224000000000000000000.0
250000000000000000000.0
280000000000000000000.0
320000000000000000000.0
360000000000000000000.0
400000000000000000000.0
450000000000000000000.0
500000000000000000000.0
560000000000000000000.0
630000000000000000000.0
710000000000000000000.0
800000000000000000000.0
900000000000000000000.0
1000000000000000000000.0
1120000000000000000000.0
1250000000000000000000.0
1400000000000000000000.0
1600000000000000000000.0
1800000000000000000000.0
2000000000000000000000.0
2240000000000000000000.0
2500000000000000000000.0
2800000000000000000000.0
3200000000000000000000.0
3600000000000000000000.0
4000000000000000000000.0
4500000000000000000000.0
5000000000000000000000.0
5600000000000000000000.0
6300000000000000000000.0
7100000000000000000000.0
8000000000000000000000.0
9000000000000000000000.0
10000000000000000000000.0
11200000000000000000000.0
12500000000000000000000.0
14000000000000000000000.0
16000000000000000000000.0
18000000000000000000000.0
20000000000000000000000.0
22400000000000000000000.0
25000000000000000000000.0
28000000000000000000000.0
32000000000000000000000.0
36000000000000000000000.0
40000000000000000000000.0
45000000000000000000000.0
50000000000000000000000.0
56000000000000000000000.0
63000000000000000000000.0
71000000000000000000000.0
80000000000000000000000.0
90000000000000000000000.0
100000000000000000000000.0
112000000000000000000000.0
125000000000000000000000.0
140000000000000000000000.0
160000000000000000000000.0
180000000000000000000000.0
200000000000000000000000.0
224000000000000000000000.0
250000000000000000000000.0
280000000000000000000000.0
320000000000000000000000.0
360000000000000000000000.0
400000000000000000000000.0
450000000000000000000000.0
500000000000000000000000.0
560000000000000000000000.0
630000000000000000000000.0
710000000000000000000000.0
800000000000000000000000.0
900000000000000000000000.0
1000000000000000000000000.0
1120000000000000000000000.0
1250000000000000000000000.0
1400000000000000000000000.0
1600000000000000000000000.0
1800000000000000000000000.0
2000000000000000000000000.0
2240000000000000000000000.0
2500000000000000000000000.0
2800000000000000000000000.0
3200000000000000000000000.0
3600000000000000000000000.0
4000000000000000000000000.0
4500000000000000000000000.0
5000000000000000000000000.0
5600000000000000000000000.0
6300000000000000000000000.0
7100000000000000000000000.0
8000000000000000000000000.0
9000000000000000000000000.0
10000000000000000000000000.0
11200000000000000000000000.0
12500000000000000000000000.0
14000000000000000000000000.0
16000000000000000000000000.0
18000000000000000000000000.0
20000000000000000000000000.0
22400000000000000000000000.0
25000000000000000000000000.0
28000000000000000000000000.0
32000000000000000000000000.0
36000000000000000000000000.0
40000000000000000000000000.0
45000000000000000000000000.0
50000000000000000000000000.0
56000000000000000000000000.0
63000000000000000000000000.0
71000000000000000000000000.0
80000000000000000000000000.0
90000000000000000000000000.0
100000000000000000000000000.0
112000000000000000000000000.0
125000000000000000000000000.0
140000000000000000000000000.0
160000000000000000000000000.0
180000000000000000000000000.0
200000000000000000000000000.0
224000000000000000000000000.0
250000000000000000000000000.0
280000000000000000000000000.0
320000000000000000000000000.0
360000000000000000000000000.0
400000000000000000000000000.0
450000000000000000000000000.0
500000000000000000000000000.0
560000000000000000000000000.0
630000000000000000000000000.0
710000000000000000000000000.0
800000000000000000000000000.0
900000000000000000000000000.0
1000000000000000000000000000.0
1120000000000000000000000000.0
1250000000000000000000000000.0
1400000000000000000000000000.0
1600000000000000000000000000.0
1800000000000000000000000000.0
2000000000000000000000000000.0
2240000000000000000000000000.0
2500000000000000000000000000.0
2800000000000000000000000000.0
3200000000000000000000000000.0
3600000000000000000000000000.0
4000000000000000000000000000.0
4500000000000000000000000000.0
5000000000000000000000000000.0
5600000000000000000000000000.0
6300000000000000000000000000.0
7100000000000000000000000000.0
8000000000000000000000000000.0
9000000000000000000000000000.0
10000000000000000000000000000.0
11200000000000000000000000000.0
12500000000000000000000000000.0
14000000000000000000000000000.0
16000000000000000000000000000.0
18000000000000000000000000000.0
20000000000000000000000000000.0
22400000000000000000000000000.0
25000000000000000000000000000.0
28000000000000000000000000000.0
32000000000000000000000000000.0
36000000000000000000000000000.0
40000000000000000000000000000.0
45000000000000000000000000000.0
50000000000000000000000000000.0
56000000000000000000000000000.0
63000000000000000000000000000.0
71000000000000000000000000000.0
80000000000000000000000000000.0
90000000000000000000000000000.0
100000000000000000000000000000.0
112000000000000000000000000000.0
125000000000000000000000000000.0
140000000000000000000000000000.0
160000000000000000000000000000.0
180000000000000000000000000000.0
200000000000000000000000000000.0
224000000000000000000000000000.0
250000000000000000000000000000.0
280000000000000000000000000000.0
320000000000000000000000000000.0
360000000000000000000000000000.0
400000000000000000000000000000.0
450000000000000000000000000000.0
500000000000000000000000000000.0
560000000000000000000000000000.0
630000000000000000000000000000.0
710000000000000000000000000000.0
800000000000000000000000000000.0
900000000000000000000000000000.0
1000000000000000000000000000000.0
1120000000000000000000000000000.0
1250000000000000000000000000000.0
1400000000000000000000000000000.0
1600000000000000000000000000000.0
1800000000000000000000000000000.0
2000000000000000000000000000000.0
2240000000000000000000000000000.0
2500000000000000000000000000000.0
2800000000000000000000000000000.0
3200000000000000000000000000000.0
3600000000000000000000000000000.0
4000000000000000000000000000000.0
4500000000000000000000000000000.0
5000000000000000000000000000000.0
5600000000000000000000000000000.0
6300000000000000000000000000000.0
7100000000000000000000000000000.0
8000000000000000000000000000000.0
9000000000000000000000000000000.0
10000000000000000000000000000000.0
11200000000000000000000000000000.0
12500000000000000000000000000000.0
14000000000000000000000000000000.0
16000000000000000000000000000000.0
18000000000000000000000000000000.0
20000000000000000000000000000000.0
22400000000000000000000000000000.0
25000000000000000000000000000000.0
28000000000000000000000000000000.0
32000000000000000000000000000000.0
36000000000000000000000000000000.0
40000000000000000000000000000000.0
45000000000000000000000000000000.0
50000000000000000000000000000000.0
56000000000000000000000000000000.0
63000000000000000000000000000000.0
71000000000000000000000000000000.0
80000000000000000000000000000000.0
90000000000000000000000000000000.0
100000000000000000000000000000000.0
112000000000000000000000000000000.0
125000000000000000000000000000000.0
140000000000000000000000000000000.0
160000000000000000000000000000000.0
180000000000000000000000000000000.0
200000000000000000000000000000000.0
224000000000000000000000000000000.0
250000000000000000000000000000000.0
280000000000000000000000000000000.0
320000000000000000000000000000000.0
360000000000000000000000000000000.0
400000000000000000000000000000000.0
450000000000000000000000000000000.0
500000000000000000000000000000000.0
560000000000000000000000000000000.0
630000000000000000000000000000000.0
710000000000000000000000000000000.0
800000000000000000000000000000000.0
900000000000000000000000000000000.0
1000000000000000000000000000000000.0
1120000000000000000000000000000000.0
1250000000000000000000000000000000.0
1400000000000000000000000000000000.0
1600000000000000000000000000000000.0
1800000000000000000000000000000000.0
2000000000000000000000000000000000.0
2240000000000000000000000000000000.0
2500000000000000000000000000000000.0
2800000000000000000000000000000000.0
3200000000000000000000000000000000.0
3600000000000000000000000000000000.0
4000000000000000000000000000000000.0
4500000000000000000000000000000000.0
5000000000000000000000000000000000.0
5600000000000000000000000000000000.0
6300000000000000000000000000000000.0
7100000000000000000000000000000000.0
8000000000000000000000000000000000.0
9000000000000000000000000000000000.0
10000000000000000000000000000000000.0
11200000000000000000000000000000000.0
12500000000000000000000000000000000.0
14000000000000000000000000000000000.0
16000000000000000000000000000000000.0
18000000000000000000000000000000000.0
20000000000000000000000000000000000.0
22400000000000000000000000000000000.0
25000000000000000000000000000000000.0
28000000000000000000000000000000000.0
32000000000000000000000000000000000.0
36000000000000000000000000000000000.0
40000000000000000000000000000000000.0
45000000000000000000000000000000000.0
50000000000000000000000000000000000.0
56000000000000000000000000000000000.0
63000000000000000000000000000000000.0
71000000000000000000000000000000000.0
80000000000000000000000000000000000.0
90000000000000000000000000000000000.0
100000000000000000000000000000000000.0
112000000000000000000000000000000000.0
125000000000000000000000000000000000.0
140000000000000000000000000000000000.0
160000000000000000000000000000000000.0
180000000000000000000000000000000000.0
200000000000000000000000000000000000.0
224000000000000000000000000000000000.0
250000000000000000000000000000000000.0
280000000000000000000000000000000000.0
320000000000000000000000000000000000.0
360000000000000000000000000000000000.0
400000000000000000000000000000000000.0
450000000000000000000000000000000000.0
500000000000000000000000000000000000.0
560000000000000000000000000000000000.0
630000000000000000000000000000000000.0
710000000000000000000000000000000000.0
800000000000000000000000000000000000.0
900000000000000000000000000000000000.0
1000000000000000000000000000000000000.0
1120000000000000000000000000000000000.0
1250000000000000000000000000000000000.0
1400000000000000000000000000000000000.0
1600000000000000000000000000000000000.0
1800000000000000000000000000000000000.0
2000000000000000000000000000000000000.0
2240000000000000000000000000000000000.0
2500000000000000000000000000000000000.0
2800000000000000000000000000000000000.0
3200000000000000000000000000000000000.0
3600000000000000000000000000000000000.0
4000000000000000000000000000000000000.0
4500000000000000000000000000000000000.0
5000000000000000000000000000000000000.0
5600000000000000000000000000000000000.0
6300000000000000000000000000000000000.0
7100000000000000000000000000000000000.0
8000000000000000000000000000000000000.0
9000000000000000000000000000000000000.0
10000000000000000000000000000000000000.0
11200000000000000000000000000000000000.0
12500000000000000000000000000000000000.0
14000000000000000000000000000000000000.0
16000000000000000000000000000000000000.0
18000000000000000000000000000000000000.0
20000000000000000000000000000000000000.0
22400000000000000000000000000000000000.0
25000000000000000000000000000000000000.0
28000000000000000000000000000000000000.0
32000000000000000000000000000000000000.0
36000000000000000000000000000000000000.0
40000000000000000000000000000000000000.0
45000000000000000000000000000000000000.0
50000000000000000000000000000000000000.0
56000000000000000000000000000000000000.0
63000000000000000000000000000000000000.0
71000000000000000000000000000000000000.0
80000000000000000000000000000000000000.0
90000000000000000000000000000000000000.0
100000000000000000000000000000000000000.0
112000000000000000000000000000000000000.0
125000000000000000000000000000000000000.0
140000000000000000000000000000000000000.0
160000000000000000000000000000000000000.0
180000000000000000000000000000000000000.0
200000000000000000000000000000000000000.0
224000000000000000000000000000000000000.0
250000000000000000000000000000000000000.0
280000000000000000000000000000000000000.0
320000000000000000000000000000000000000.0
360000000000000000000000000000000000000.0
400000000000000000000000000000000000000.0
450000000000000000000000000000000000000.0
500000000000000000000000000000000000000.0
560000000000000000000000000000000000000.0
630000000000000000000000000000000000000.0
710000000000000000000000000000000000000.0
800000000000000000000000000000000000000.0
900000000000000000000000000000000000000.0
1000000000000000000000000000000000000000.0
1120000000000000000000000000000000000000.0
1250000000000000000000000000000000000000.0
1400000000000000000000000000000000000000.0
1600000000000000000000000000000000000000.0
1800000000000000000000000000000000000000.0
2000000000000000000000000000000000000000.0
2240000000000000000000000000000000000000.0
2500000000000000000000000000000000000000.0
2800000000000000000000000000000000000000.0
3200000000000000000000000000000000000000.0
3600000000000000000000000000000000000000.0
4000000000000000000000000000000000000000.0
4500000000000000000000000000000000000000.0
5000000000000000000000000000000000000000.0
5600000000000000000000000000000000000000.0
6300000000000000000000000000000000000000.0
7100000000000000000000000000000000000000.0
8000000000000000000000000000000000000000.0
9000000000000000000000000000000000000000.0
10000000000000000000000000000000000000000.0
11200000000000000000000000000000000000000.0
12500000000000000000000000000000000000000.0
14000000000000000000000000000000000000000.0
16000000000000000000000000000000000000000.0
18000000000000000000000000000000000000000.0
20000000000000000000000000000000000000000.0
22400000000000000000000000000000000000000.0
25000000000000000000000000000000000000000.0
28000000000000000000000000000000000000000.0
32000000000000000000000000000000000000000.0
36000000000000000000000000000000000000000.0
40000000000000000000000000000000000000000.0
45000000000000000000000000000000000000000.0
50000000000000000000000000000000000000000.0
56000000000000000000000000000000000000000.0
63000000000000000000000000000000000000000.0
71000000000000000000000000000000000000000.0
80000000000000000000000000000000000000000.0
90000000000000000000000000000000000000000.0
100000000000000000000000000000000000000000.0
112000000000000000000000000000000000000000.0
125000000000000000000000000000000000000000.0
140000000000000000000000000000000000000000.0
160000000000000000000000000000000000000000.0
180000000000000000000000000000000000000000.0
200000000000000000000000000000000000000000.0
224000000000000000000000000000000000000000.0
250000000000000000000000000000000000000000.0
280000000000000000000000000000000000000000.0
320000000000000000000000000000000000000000.0
360000000000000000000000000000000000000000.0
400000000000000000000000000000000000000000.0
450000000000000000000000000000000000000000.0
500000000000000000000000000000000000000000.0
560000000000000000000000000000000000000000.0
630000000000000000000000000000000000000000.0
710000000000000000000000000000000000000000.0
800000000000000000000000000000000000000000.0
900000000000000000000000000000000000000000.0
1000000000000000000000000000000000000000000.0
1120000000000000000000000000000000000000000.0
1250000000000000000000000000000000000000000.0
1400000000000000000000000000000000000000000.0
1600000000000000000000000000000000000000000.0
1800000000000000000000000000000000000000000.0
2000000000000000000000000000000000000000000.0
2240000000000000000000000000000000000000000.0
2500000000000000000000000000000000000000000.0
2800000000000000000000000000000000000000000.0
3200000000000000000000000000000000000000000.0
3600000000000000000000000000000000000000000.0
4000000000000000000000000000000000000000000.0
4500000000000000000000000000000000000000000.0
5000000000000000000000000000000000000000000.0
5600000000000000000000000000000000000000000.0
6300000000000000000000000000000000000000000.0
7100000000000000000000000000000000000000000.0
8000000000000000000000000000000000000000000.0
9000000000000000000000000000000000000000000.0
10000000000000000000000000000000000000000000.0
11200000000000000000000000000000000000000000.0
12500000000000000000000000000000000000000000.0
14000000000000000000000000000000000000000000.0
16000000000000000000000000000000000000000000.0
18000000000000000000000000000000000000000000.0
20000000000000000000000000000000000000000000.0
22400000000000000000000000000000000000000000.0
25000000000000000000000000000000000000000000.0
28000000000000000000000000000000000000000000.0
32000000000000000000000000000000000000000000.0
36000000000000000000000000000000000000000000.0
40000000000000000000000000000000000000000000.0
45000000000000000000000000000000000000000000.0
50000000000000000000000000000000000000000000.0
56000000000000000000000000000000000000000000.0
63000000000000000000000000000000000000000000.0
71000000000000000000000000000000000000000000.0
80000000000000000000000000000000000000000000.0
90000000000000000000000000000000000000000000.0
100000000000000000000000000000000000000000000.0
112000000000000000000000000000000000000000000.0
125000000000000000000000000000000000000000000.0
140000000000000000000000000000000000000000000.0
160000000000000000000000000000000000000000000.0
180000000000000000000000000000000000000000000.0
200000000000000000000000000000000000000000000.0
224000000000000000000000000000000000000000000.0
250000000000000000000000000000000000000000000.0
280000000000000000000000000000000000000000000.0
320000000000000000000000000000000000000000000.0
360000000000000000000000000000000000000000000.0
400000000000000000000000000000000000000000000.0
450000000000000000000000000000000000000000000.0
500000000000000000000000000000000000000000000.0
560000000000000000000000000000000000000000000.0
630000000000000000000000000000000000000000000.0
710000000000000000000000000000000000000000000.0
800000000000000000000000000000000000000000000.0
900000000000000000000000000000000000000000000.0
1000000000000000000000000000000000000000000000.0
1120000000000000000000000000000000000000000000.0
1250000000000000000000000000000000000000000000.0
1400000000000000000000000000000000000000000000.0
1600000000000000000000000000000000000000000000.0
1800000000000000000000000000000000000000000000.0
2000000000000000000000000000000000000000000000.0
2240000000000000000000000000000000000000000000.0
2500000000000000000000000000000000000000000000.0
2800000000000000000000000000000000000000000000.0
3200000000000000000000000000000000000000000000.0
3600000000000000000000000000000000000000000000.0
4000000000000000000000000000000000000000000000.0
4500000000000000000000000000000000000000000000.0
5000000000000000000000000000000000000000000000.0
5600000000000000000000000000000000000000000000.0
6300000000000000000000000000000000000000000000.0
7100000000000000000000000000000000000000000000.0
8000000000000000000000000000000000000000000000.0
9000000000000000000000000000000000000000000000.0
10000000000000000000000000000000000000000000000.0
11200000000000000000000000000000000000000000000.0
12500000000000000000000000000000000000000000000.0
14000000000000000000000000000000000000000000000.0
16000000000000000000000000000000000000000000000.0
18000000000000000000000000000000000000000000000.0
20000000000000000000000000000000000000000000000.0
22400000000000000000000000000000000000000000000.0
25000000000000000000000000000000000000000000000.0
28000000000000000000000000000000000000000000000.0
32000000000000000000000000000000000000000000000.0
36000000000000000000000000000000000000000000000.0
40000000000000000000000000000000000000000000000.0
45000000000000000000000000000000000000000000000.0
50000000000000000000000000000000000000000000000.0
56000000000000000000000000000000000000000000000.0
63000000000000000000000000000000000000000000000.0
71000000000000000000000000000000000000000000000.0
80000000000000000000000000000000000000000000000.0
90000000000000000000000000000000000000000000000.0
100000000000000000000000000000000000000000000000.0
112000000000000000000000000000000000000000000000.0
125000000000000000000000000000000000000000000000.0
140000000000000000000000000000000000000000000000.0
160000000000000000000000000000000000000000000000.0
180000000000000000000000000000000000000000000000.0
200000000000000000000000000000000000000000000000.0
224000000000000000000000000000000000000000000000.0
250000000000000000000000000000000000000000000000.0
280000000000000000000000000000000000000000000000.0
320000000000000000000000000000000000000000000000.0
360000000000000000000000000000000000000000000000.0
400000000000000000000000000000000000000000000000.0
450000000000000000000000000000000000000000000000.0
500000000000000000000000000000000000000000000000.0
560000000000000000000000000000000000000000000000.0
630000000000000000000000000000000000000000000000.0
710000000000000000000000000000000000000000000000.0
800000000000000000000000000000000000000000000000.0
900000000000000000000000000000000000000000000000.0
1000000000000000000000000000000000000000000000000.0
1120000000000000000000000000000000000000000000000.0
1250000000000000000000000000000000000000000000000.0
1400000000000000000000000000000000000000000000000.0
1600000000000000000000000000000000000000000000000.0
1800000000000000000000000000000000000000000000000.0
2000000000000000000000000000000000000000000000000.0
2240000000000000000000000000000000000000000000000.0
2500000000000000000000000000000000000000000000000.0
2800000000000000000000000000000000000000000000000.0
3200000000000000000000000000000000000000000000000.0
3600000000000000000000000000000000000000000000000.0
4000000000000000000000000000000000000000000000000.0
4500000000000000000000000000000000000000000000000.0
5000000000000000000000000000000000000000000000000.0
5600000000000000000000000000000000000000000000000.0
6300000000000000000000000000000000000000000000000.0
7100000000000000000000000000000000000000000000000.0
8000000000000000000000000000000000000000000000000.0
9000000000000000000000000000000000000000000000000.0
10000000000000000000000000000000000000000000000000.0
11200000000000000000000000000000000000000000000000.0
12500000000000000000000000000000000000000000000000.0
14000000000000000000000000000000000000000000000000.0
16000000000000000000000000000000000000000000000000.0
18000000000000000000000000000000000000000000000000.0
20000000000000000000000000000000000000000000000000.0
22400000000000000000000000000000000000000000000000.0
25000000000000000000000000000000000000000000000000.0
28000000000000000000000000000000000000000000000000.0
32000000000000000000000000000000000000000000000000.0
36000000000000000000000000000000000000000000000000.0
40000000000000000000000000000000000000000000000000.0
45000000000000000000000000000000000000000000000000.0
50000000000000000000000000000000000000000000000000.0
56000000000000000000000000000000000000000000000000.0
63000000000000000000000000000000000000000000000000.0
71000000000000000000000000000000000000000000000000.0
80000000000000000000000000000000000000000000000000.0
90000000000000000000000000000000000000000000000000.0
100000000000000000000000000000000000000000000000000.0
112000000000000000000000000000000000000000000000000.0
125000000000000000000000000000000000000000000000000.0
140000000000000000000000000000000000000000000000000.0
160000000000000000000000000000000000000000000000000.0
180000000000000000000000000000000000000000000000000.0
200000000000000000000000000000000000000000000000000.0
224000000000000000000000000000000000000000000000000.0
250000000000000000000000000000000000000000000000000.0
280000000000000000000000000000000000000000000000000.0
320000000000000000000000000000000000000000000000000.0
360000000000000000000000000000000000000000000000000.0
400000000000000000000000000000000000000000000000000.0
450000000000000000000000000000000000000000000000000.0
500000000000000000000000000000000000000000000000000.0
560000000000000000000000000000000000000000000000000.0
630000000000000000000000000000000000000000000000000.0
710000000000000000000000000000000000000000000000000.0
800000000000000000000000000000000000000000000000000.0
900000000000000000000000000000000000000000000000000.0
1000000000000000000000000000000000000000000000000000.0
1120000000000000000000000000000000000000000000000000.0
1250000000000000000000000000000000000000000000000000.0
1400000000000000000000000000000000000000000000000000.0
1600000000000000000000000000000000000000000000000000.0
1800000000000000000000000000000000000000000000000000.0
2000000000000000000000000000000000000000000000000000.0
2240000000000000000000000000000000000000000000000000.0
2500000000000000000000000000000000000000000000000000.0
2800000000000000000000000000000000000000000000000000.0
3200000000000000000000000000000000000000000000000000.0
3600000000000000000000000000000000000000000000000000.0
4000000000000000000000000000000000000000000000000000.0
4500000000000000000000000000000000000000000000000000.0
5000000000000000000000000000000000000000000000000000.0
5600000000000000000000000000000000000000000000000000.0
6300000000000000000000000000000000000000000000000000.0
7100000000000000000000000000000000000000000000000000.0
8000000000000000000000000000000000000000000000000000.0
9000000000000000000000000000000000000000000000000000.0
10000000000000000000000000000000000000000000000000000.0
11200000000000000000000000000000000000000000000000000.0
12500000000000000000000000000000000000000000000000000.0
14000000000000000000000000000000000000000000000000000.0
16000000000000000000000000000000000000000000000000000.0
18000000000000000000000000000000000000000000000000000.0
20000000000000000000000000000000000000000000000000000.0
22400000000000000000000000000000000000000000000000000.0
25000000000000000000000000000000000000000000000000000.0
28000000000000000000000000000000000000000000000000000.0
32000000000000000000000000000000000000000000000000000.0
36000000000000000000000000000000000000000000000000000.0
40000000000000000000000000000000000000000000000000000.0
45000000000000000000000000000000000000000000000000000.0
50000000000000000000000000000000000000000000000000000.0
56000000000000000000000000000000000000000000000000000.0
63000000000000000000000000000000000000000000000000000.0
71000000000000000000000000000000000000000000000000000.0
80000000000000000000000000000000000000000000000000000.0
90000000000000000000000000000000000000000000000000000.0
100000000000000000000000000000000000000000000000000000.0
112000000000000000000000000000000000000000000000000000.0
125000000000000000000000000000000000000000000000000000.0
140000000000000000000000000000000000000000000000000000.0
160000000000000000000000000000000000000000000000000000.0
180000000000000000000000000000000000000000000000000000.0
200000000000000000000000000000000000000000000000000000.0
224000000000000000000000000000000000000000000000000000.0
250000000000000000000000000000000000000000000000000000.0
280000000000000000000000000000000000000000000000000000.0
320000000000000000000000000000000000000000000000000000.0
360000000000000000000000000000000000000000000000000000.0
400000000000000000000000000000000000000000000000000000.0
450000000000000000000000000000000000000000000000000000.0
500000000000000000000000000000000000000000000000000000.0
560000000000000000000000000000000000000000000000000000.0
630000000000000000000000000000000000000000000000000000.0
710000000000000000000000000000000000000000000000000000.0
800000000000000000000000000000000000000000000000000000.0
900000000000000000000000000000000000000000000000000000.0
1000000000000000000000000000000000000000000000000000000.0
1120000000000000000000000000000000000000000000000000000.0
1250000000000000000000000000000000000000000000000000000.0
1400000000000000000000000000000000000000000000000000000.0
1600000000000000000000000000000000000000000000000000000.0
1800000000000000000000000000000000000000000000000000000.0
2000000000000000000000000000000000000000000000000000000.0
2240000000000000000000000000000000000000000000000000000.0
2500000000000000000000000000000000000000000000000000000.0
2800000000000000000000000000000000000000000000000000000.0
3200000000000000000000000000000000000000000000000000000.0
3600000000000000000000000000000000000000000000000000000.0
4000000000000000000000000000000000000000000000000000000.0
4500000000000000000000000000000000000000000000000000000.0
5000000000000000000000000000000000000000000000000000000.0
5600000000000000000000000000000000000000000000000000000.0
6300000000000000000000000000000000000000000000000000000.0
7100000000000000000000000000000000000000000000000000000.0
8000000000000000000000000000000000000000000000000000000.0
9000000000000000000000000000000000000000000000000000000.0
10000000000000000000000000000000000000000000000000000000.0
11200000000000000000000000000000000000000000000000000000.0
12500000000000000000000000000000000000000000000000000000.0
14000000000000000000000000000000000000000000000000000000.0
16000000000000000000000000000000000000000000000000000000.0
18000000000000000000000000000000000000000000000000000000.0
20000000000000000000000000000000000000000000000000000000.0
22400000000000000000000000000000000000000000000000000000.0
25000000000000000000000000000000000000000000000000000000.0
28000000000000000000000000000000000000000000000000000000.0
32000000000000000000000000000000000000000000000000000000.0
36000000000000000000000000000000000000000000000000000000.0
40000000000000000000000000000000000000000000000000000000.0
45000000000000000000000000000000000000000000000000000000.0
50000000000000000000000000000000000000000000000000000000.0
56000000000000000000000000000000000000000000000000000000.0
63000000000000000000000000000000000000000000000000000000.0
71000000000000000000000000000000000000000000000000000000.0
80000000000000000000000000000000000000000000000000000000.0
90000000000000000000000000000000000000000000000000000000.0
100000000000000000000000000000000000000000000000000000000.0
112000000000000000000000000000000000000000000000000000000.0
125000000000000000000000000000000000000000000000000000000.0
140000000000000000000000000000000000000000000000000000000.0
160000000000000000000000000000000000000000000000000000000.0
180000000000000000000000000000000000000000000000000000000.0
200000000000000000000000000000000000000000000000000000000.0
224000000000000000000000000000000000000000000000000000000.0
250000000000000000000000000000000000000000000000000000000.0
280000000000000000000000000000000000000000000000000000000.0
320000000000000000000000000000000000000000000000000000000.0
360000000000000000000000000000000000000000000000000000000.0
400000000000000000000000000000000000000000000000000000000.0
450000000000000000000000000000000000000000000000000000000.0
500000000000000000000000000000000000000000000000000000000.0
560000000000000000000000000000000000000000000000000000000.0
630000000000000000000000000000000000000000000000000000000.0
710000000000000000000000000000000000000000000000000000000.0
800000000000000000000000000000000000000000000000000000000.0
900000000000000000000000000000000000000000000000000000000.0
1000000000000000000000000000000000000000000000000000000000.0
1120000000000000000000000000000000000000000000000000000000.0
1250000000000000000000000000000000000000000000000000000000.0
1400000000000000000000000000000000000000000000000000000000.0
1600000000000000000000000000000000000000000000000000000000.0
1800000000000000000000000000000000000000000000000000000000.0
2000000000000000000000000000000000000000000000000000000000.0
2240000000000000000000000000000000000000000000000000000000.0
2500000000000000000000000000000000000000000000000000000000.0
2800000000000000000000000000000000000000000000000000000000.0
3200000000000000000000000000000000000000000000000000000000.0
3600000000000000000000000000000000000000000000000000000000.0
4000000000000000000000000000000000000000000000000000000000.0
4500000000000000000000000000000000000000000000000000000000.0
5000000000000000000000000000000000000000000000000000000000.0
5600000000000000000000000000000000000000000000000000000000.0
6300000000000000000000000000000000000000000000000000000000.0
7100000000000000000000000000000000000000000000000000000000.0
8000000000000000000000000000000000000000000000000000000000.0
9000000000000000000000000000000000000000000000000000000000.0
10000000000000000000000000000000000000000000000000000000000.0
11200000000000000000000000000000000000000000000000000000000.0
12500000000000000000000000000000000000000000000000000000000.0
14000000000000000000000000000000000000000000000000000000000.0
16000000000000000000000000000000000000000000000000000000000.0
18000000000000000000000000000000000000000000000000000000000.0
20000000000000000000000000000000000000000000000000000000000.0
22400000000000000000000000000000000000000000000000000000000.0
25000000000000000000000000000000000000000000000000000000000.0
28000000000000000000000000000000000000000000000000000000000.0
32000000000000000000000000000000000000000000000000000000000.0
36000000000000000000000000000000000000000000000000000000000.0
40000000000000000000000000000000000000000000000000000000000.0
45000000000000000000000000000000000000000000000000000000000.0
50000000000000000000000000000000000000000000000000000000000.0
56000000000000000000000000000000000000000000000000000000000.0
63000000000000000000000000000000000000000000000000000000000.0
71000000000000000000000000000000000000000000000000000000000.0
80000000000000000000000000000000000000000000000000000000000.0
90000000000000000000000000000000000000000000000000000000000.0
100000000000000000000000000000000000000000000000000000000000.0
112000000000000000000000000000000000000000000000000000000000.0
125000000000000000000000000000000000000000000000000000000000.0
140000000000000000000000000000000000000000000000000000000000.0
160000000000000000000000000000000000000000000000000000000000.0
180000000000000000000000000000000000000000000000000000000000.0
200000000000000000000000000000000000000000000000000000000000.0
224000000000000000000000000000000000000000000000000000000000.0
250000000000000000000000000000000000000000000000000000000000.

UNCLASSIFIED

SECURITY CLASSIFICATION OF THIS PAGE

REPORT DOCUMENTATION PAGE

1a. REPORT SECURITY CLASSIFICATION UNCLASSIFIED	1b. RESTRICTIVE MARKINGS
2a. SECURITY CLASSIFICATION AUTHORITY	3. DISTRIBUTION/AVAILABILITY OF REPORT Approved for public release; distribution unlimited
2b. DECLASSIFICATION/DOWNGRADING SCHEDULE	
4. PERFORMING ORGANIZATION REPORT NUMBER(S) AFIT/GAE/ENY/83D-5	5. MONITORING ORGANIZATION REPORT NUMBER(S)
6a. NAME OF PERFORMING ORGANIZATION School of Engineering AF Institute of Technology 6b. OFFICE SYMBOL (If applicable) AFIT/EN	7a. NAME OF MONITORING ORGANIZATION
6c. ADDRESS (City, State and ZIP Code) Wright-Patterson AFB, Ohio 45433	7b. ADDRESS (City, State and ZIP Code)
8a. NAME OF FUNDING/SPONSORING ORGANIZATION 8b. OFFICE SYMBOL (If applicable)	9. PROCUREMENT INSTRUMENT IDENTIFICATION NUMBER
8c. ADDRESS (City, State and ZIP Code)	10. SOURCE OF FUNDING NOS. PROGRAM ELEMENT NO. / PROJECT NO. / TASK NO. / WORK UNIT NO.
11. TITLE (Include Security Classification) See box 19	
12. PERSONAL AUTHOR(S) Gary F. Clark, B.S., Capt, USAF	
13a. TYPE OF REPORT MS Thesis 13b. TIME COVERED FROM _____ TO _____	14. DATE OF REPORT (Yr., Mo., Day) 1983 December 15. PAGE COUNT 97
16. SUPPLEMENTARY NOTATION 3 JAN 1984 Approved for public release: IAW AFR 190-17. LYNN E. WOLAVER Dean for Research and Professional Development Air Force Institute of Technology (AFIT) Wright-Patterson AFB OH 45433	
17. COSATI CODES FIELD: 20 / GROUP: 04 / SUB. GR.	18. SUBJECT TERMS (Continue on reverse if necessary and identify by block number) vortex street, water tunnel free jet, vortex shedding water table, circular cylinder

19. ABSTRACT (Continue on reverse if necessary and identify by block number)

Title: EFFECTS OF MULTIPLE CYLINDERS ON THE FORMATION OF VON KARMAN VORTEX STREETS

Thesis Advisor: Eric J. Jumper, Maj, USAF

20. DISTRIBUTION/AVAILABILITY OF ABSTRACT UNCLASSIFIED/UNLIMITED ☒ SAME AS RPT. ☐ DTIC USERS ☐	21. ABSTRACT SECURITY CLASSIFICATION UNCLASSIFIED
22a. NAME OF RESPONSIBLE INDIVIDUAL Eric J. Jumper, Major, USAF	22b. TELEPHONE NUMBER (Include Area Code) 513-255-2998 22c. OFFICE SYMBOL AFIT/ENY

DD FORM 1473, 83 APR EDITION OF 1 JAN 73 IS OBSOLETE.

UNCLASSIFIED

SECURITY CLASSIFICATION OF THIS PAGE

19.

This study investigated the effect of multiple cylinders positioned within 6 diameters on the formation of von Kármán vortex streets. This research effort used a water tunnel and a modified free jet to create desired flow conditions. Both flow visualization and hot film data were obtained under various conditions.

Circular cylinders were used as models for the creation of the vortex street. A water table was modified into a water tunnel which was run at various flow velocities to produce flow conditions at $Re_D \leq 1 \times 10^4$. Shadowgraph-type photos were taken of the water flow field. A free jet was run at various flow velocities to produce flow conditions at a higher Re_D. A diverging dead-wake pattern was created by .794 cm diameter rods placed at the exit of a 1 cm by 10 cm free jet at M = .1 and .6. Classical vortex streets were created using the same size cylinder and a 5 cm by 5 cm free jet nozzle with an attached channel. Both schlieren photographs and hot film measurements were taken of the flow fields at $Re_D = 1.1 \times 10^5$ and 1.88×10^4 respectively.

The water tunnel results indicate the formation of the von Kármán vortex street has no dependence on either the absence or presence of other cylinders. The free jet data confirmed the water tunnel results and showed that dependence of the von Kármán vortex street in the gas flow facility used in this study was due to jet conditioning and ultimately could be produced for this size cylinder in a duct (i.e. in closed tunnel surroundings). Diverging dead-wake patterns were formed when no duct was present. Statistical hot film data taken at M = .1 substantiated these results.